

# CHARACTERIZATION OF PHOTOTOXICITY REACTIONS IN HUMAN AND ANIMAL SKIN MODELS

**Inauguraldissertation**

zur

Erlangung der Würde eines Doktors der Philosophie

vorgelegt der

Philosophisch-Naturwissenschaftlichen Fakultät der Universität Basel

Von

**Stéphanie Boudon**

aus Frankreich

Basel, 2013

Original document stored on the publication server of the University of Basel

**[edoc.unibas.ch](http://edoc.unibas.ch)**



This work is licenced under the agreement „Attribution Non-Commercial No Derivatives – 2.5  
Switzerland“. The complete text may be viewed here:

**[creativecommons.org/licenses/by-nc-nd/2.5/ch/deed.en](http://creativecommons.org/licenses/by-nc-nd/2.5/ch/deed.en)**

Genehmigt von der Philosophisch-Naturwissenschaftlichen Fakultät  
auf Antrag von

Prof. Dr. Alex Odermatt

Dr. Daniel Bauer

Prof. Dr. med. Stephan Krähenbühl

Basel, den 10 Dezember 2013.

Prof. Dr. Jörg Schibler  
Dekan



## Namensnennung-Keine kommerzielle Nutzung-Keine Bearbeitung 2.5 Schweiz

---

**Sie dürfen:**



das Werk vervielfältigen, verbreiten und öffentlich zugänglich machen

**Zu den folgenden Bedingungen:**



**Namensnennung.** Sie müssen den Namen des Autors/Rechteinhabers in der von ihm festgelegten Weise nennen (wodurch aber nicht der Eindruck entstehen darf, Sie oder die Nutzung des Werkes durch Sie würden entlohnt).



**Keine kommerzielle Nutzung.** Dieses Werk darf nicht für kommerzielle Zwecke verwendet werden.



**Keine Bearbeitung.** Dieses Werk darf nicht bearbeitet oder in anderer Weise verändert werden.

- Im Falle einer Verbreitung müssen Sie anderen die Lizenzbedingungen, unter welche dieses Werk fällt, mitteilen. Am Einfachsten ist es, einen Link auf diese Seite einzubinden.
- Jede der vorgenannten Bedingungen kann aufgehoben werden, sofern Sie die Einwilligung des Rechteinhabers dazu erhalten.
- Diese Lizenz lässt die Urheberpersönlichkeitsrechte unberührt.

**Die gesetzlichen Schranken des Urheberrechts bleiben hiervon unberührt.**

Die Commons Deed ist eine Zusammenfassung des Lizenzvertrags in allgemeinverständlicher Sprache: <http://creativecommons.org/licenses/by-nc-nd/2.5/ch/legalcode.de>

Haftungsausschluss:

Die Commons Deed ist kein Lizenzvertrag. Sie ist lediglich ein Referenztext, der den zugrundeliegenden Lizenzvertrag übersichtlich und in allgemeinverständlicher Sprache wiedergibt. Die Deed selbst entfaltet keine juristische Wirkung und erscheint im eigentlichen Lizenzvertrag nicht. Creative Commons ist keine Rechtsanwalts-gesellschaft und leistet keine Rechtsberatung. Die Weitergabe und Verlinkung des Commons Deeds führt zu keinem Mandatsverhältnis.



*To my parents*



# Acknowledgements

*I wish to express my gratitude to Dr. Daniel Bauer for giving me the opportunity to prepare my thesis at Novartis Institute for BioMedical Research and for supervising me during this thesis.*

*I am very grateful to Prof. Alex Odermatt for accepting to be the Faculty responsible, for sharing with me his enthusiasm for Science and for his valuable help for the successful conclusion of my PhD.*

*I would like to extend my gratitude to Prof. Stephan Krähenbühl who kindly accepted to review this thesis.*

*My general thanks to Novartis Pharma AG, University of Basel and the ProDoc program for their financial and nonfinancial support.*

*My gratitude goes to Dr. Ulla Plappert for her support throughout my PhD. Thank you for your excellent support, your positive energy, and encouragement.*

*My gratitude goes to Martin Schneider. I was honored to work with you during my thesis and I am grateful for your continuous support.*

*I would like to thank Brendan Prideaux, Gregory Morandi and Dr. Markus Stoeckli from the Analytical Sciences Department at Novartis Institute for BioMedical Research for the Mass Spectrometry Imaging results.*

*I want to thank the PreClinical Safety Department at Novartis Institute for BioMedical Research. Special thanks to Monika Spielmann, Christine Blumer, Nathalie Noll, Deborah Garcia, René Schaffner, Brigitte Mueller, Philippe Scheubel and Catherine Schiltz for sharing their valuable knowledge and expertise, and above all, for the many cheerful laughs.*

*I will end by deeply thanking my family and dear friends in Switzerland and France. Their continuous support throughout all these years made this thesis not only an academic achievement but a rewarding and meaningful Life's experience.*

*I am deeply grateful to Joshua Blumer for his wholehearted support, encouragement, affection and love.*



## Summary

Phototoxicity is a relatively common phenomenon and is an adverse effect of some systemic drugs. A large number of pharmaceutical drug substances are known to carry the potential to elicit a phototoxic response (Moore 2002, Ferguson 2002). Reported cases of phototoxic responses may account for 5 to 10 % of recorded cutaneous adverse drug reactions (Selvaag 1997). As these abnormal reactions seriously limit or exclude the usage of certain drugs, it is essential to identify such liabilities early in development. Therefore, photosafety of drug candidate molecules needs to be evaluated (ICH M3 R2, 2009). Often this follows a step-wise process starting with physicochemical properties (light absorption), followed by *in vitro*, *in vivo* and/or clinical testing as suggested by each successive study. A key principle in such a tiered testing strategy is that a negative result obtained in a generally accepted and highly sensitive assay does usually not warrant further testing.

In this work, we were interested in comparing the results obtained in nonclinical models (*in vitro* and *in vivo* experiments) with the clinical signs observed in human of well-known photosensitizer. The results of our investigation of phototoxicity mechanisms are presented in three research papers published in (or submitted to) peer reviewed journals representing the core of this thesis.

Starting from an established standard model we used the modified oral UV-Local Lymph Node Assay (UV-LLNA or photo-LLNA) in Balb/c mice. We demonstrated the performance of this optimized modified murine local lymph node assay, adapted for phototoxicity assessment of

systemically applied compounds. Several clinically phototoxic reference compounds were tested in mice using a sun light simulator to establish time- and dose-dependent profiles.

In order to further investigate the phototoxic reaction, we decided to focus on one molecule. We took the example of vemurafenib, a B-Raf kinase inhibitor for the treatment of patients with unresectable or metastatic melanoma carrying the BRAFV600E mutation, commercially available since 2011. This drug was selected because the phototoxicity of this drug was discarded in preclinical testing but has been reported in clinical trial. Therefore, it became a fundamental question to understand this discrepancy. The aforementioned mouse oral UV-Local Lymph Node Assay, was used to investigate the impact of formulations, dose levels, duration of treatment and timing of irradiation. The initial studies performed as part of the non-clinical development of vemurafenib with hairless rats was compared to the current study in mice. Duration of treatment and exposure to both vemurafenib and the formal UVA dose (limited to 350 to 400 nm) was clearly exceeding the conditions we have used in our studies in mice. The most apparent difference was the spectral range of the irradiation light source (350 to 400 nm versus 320 to 700 nm). Since vemurafenib does not absorb sufficiently light above 350 nm, this difference alone can easily explain the negative earlier study result in hairless rats.

To enhance our molecular understanding of phototoxicity mechanisms, an imaging technique based on matrix-assisted laser desorption/ionization mass spectrometric (MALDI-MS) was applied to samples from mouse skin and from a human 3D skin model. Using sparfloxacin as a model compound, concentration-dependent and irradiation-dependent effects could be observed *in vitro*. Furthermore, in the aforementioned established *in vivo* phototoxicity model, time- and

irradiation dependent exposure to sparfloxacin in skin samples from mouse ears following oral treatment were demonstrated.

Taken together, these results illustrate important lessons regarding photosafety testing. First of all, they demonstrate that the modified murine UV-LLNA is suitable to support preclinical photosafety assessment of systemically applied drug candidates. Furthermore, they highlight the impact of carefully designed *in vivo* phototoxicity studies. It is apparent that duration of treatment, timing of irradiation and appropriate irradiation conditions are key parameters to ensure an appropriate sensitivity.

## References

- Ferguson, J. 2002. Photosensitivity due to drugs. *Photodermatol. Photoimmunol. Photomed.* **18**(5):262-9.
- ICH, M3 (R2). 2009. Guidance on nonclinical safety studies for the conduct of human clinical trials and marketing authorization of pharmaceuticals.  
[http://www.ich.org/fileadmin/Public\\_Web\\_Site/ICH\\_Products/Guidelines/Multidisciplinary/M3\\_R2/Step4/M3\\_R2\\_Guideline.pdf](http://www.ich.org/fileadmin/Public_Web_Site/ICH_Products/Guidelines/Multidisciplinary/M3_R2/Step4/M3_R2_Guideline.pdf).
- Moore, E.M. 2002. Drug-induced cutaneous photosensitivity. *Drug Saf.* **25**: 345-372.
- Selvaag , E. 1997. Clinical drug photosensitivity – A retrospective analysis of reports to the Norwegian Adverse Drug Reactions Committee from the years 1970-1994. *Photodermatol. Photoimmunol. Photomed.* **13**: 21-23.



# Table of Contents

<b>Summary.....</b>	<b>IX</b>
---------------------	-----------

<b>Abbreviations.....</b>	<b>XVII</b>
---------------------------	-------------

<b>1. Introduction.....</b>	<b>1</b>
-----------------------------	----------

1.1. Photosafety evaluation of pharmaceuticals.....	2
---	---

1.1.1. Photochemical properties.....	3
--------------------------------------	---

1.1.2. Tissue Distribution/Pharmacokinetics.....	3
--	---

1.1.3. Nonclinical photosafety testing.....	4
---	---

1.2. Scope of the thesis.....	6
-------------------------------	---

References.....	8
-----------------	---

<b>2. Integrated preclinical photosafety testing strategy for systemically applied pharmaceuticals.....</b>	<b>13</b>
---	-----------

Abstract.....	14
---------------	----

2.1. Introduction.....	15
------------------------	----

2.2. Materials and Methods.....	17
---------------------------------	----

2.2.1. UV/visible light absorption spectra.....	17
---	----

2.2.2. In vitro 3T3 NRU phototoxicity test.....	17
---	----

2.2.3. Mice.....	19
------------------	----

2.2.4. Treatment of mice.....	19
-------------------------------	----

2.2.5. Exposure of mice to simulated sun light.....	20
---	----

2.2.6. Erythema scoring.....	21
------------------------------	----

2.2.7. Determination of ear biopsy weights and auricular LN weights and cell counts.....	21
--	----

2.2.8. Histopathology of retina.....	22
--------------------------------------	----

2.2.9. Statistical analysis.....	22
----------------------------------	----

2.3. Results.....	23
-------------------	----

2.3.1. Clinically phototoxic reference compounds in the modified murine oral (gavage) photo-LLNA.....	23
2.3.2. Drug candidates in the modified murine systemic photo-LLNA.....	31
2.4. Discussion.....	41
2.5. Conclusion.....	45
Acknowledgements.....	46
References.....	46

### **3. Characterization of Vemurafenib Phototoxicity in a Mouse Model.....51**

Abstract.....	52
3.1. Introduction.....	53
3.2. Material and methods.....	55
3.2.1. Test compounds and positive and negative control items.....	55
3.2.2. UV-visible light absorption spectra.....	56
3.2.3. In vitro 3T3 neutral red uptake phototoxicity test.....	56
3.2.4. Animal experiments.....	58
3.2.4.1. Animal husbandry.....	58
3.2.4.2. Irradiation conditions for animal experiments.....	59
3.2.4.3. Treatment protocols and endpoints.....	59
3.2.4.3.1. Oral UV-Local Lymph Node Assay in BALB/c mice.....	59
3.2.4.3.2. Time-profile of erythema and edema formation after irradiation.....	63
3.2.4.3.3. Pharmacokinetic profile of vemurafenib in BALB/c mice.....	64
3.2.4.4. Statistical analysis .....	64
3.3. Results.....	65
3.3.1. UV-visible light absorption spectra.....	65
3.3.2. In vitro phototoxicity test results.....	66
3.3.3. Oral UV-Local Lymph Node Assay.....	67
3.3.4. Time-profile of erythema and edema formation after irradiation.....	69
3.3.5. Pharmacokinetic Profile.....	70

3.4. Discussion and Conclusion.....	71
Acknowledgements.....	74
Funding.....	74
References.....	74

## **4. Evaluation of Sparfloxacin Phototoxicity with Mass Spectrometry**

### **Imaging.....77**

Abstract.....	79
4.1. Introduction.....	80
4.2. Materials and methods.....	81
4.2.1. Human 3D skin model.....	81
4.2.2. Animal experiments.....	82
4.2.2.1. Animal husbandry.....	82
4.2.2.3. Treatment protocols.....	83
4.2.2.4. Statistical analysis.....	84
4.2.3. Mass spectrometry imaging.....	85
4.2.3.1. Preparation of tissue samples for MALDI-MSI.....	85
4.2.3.2. MALDI-MSI analysis.....	86
4.3. Results and discussion.....	87
4.3.1. Localization and quantification of sparfloxacin in vitro.....	87
4.3.2. Localization and quantification of sparfloxacin as part of an in vivo phototoxicity study in mice.....	87
4.4. Conclusion.....	93
Acknowledgements.....	93
References.....	93

## **5. Conclusion and Perspectives.....95**



# Abbreviations

3D	Three-dimensional
8-MOP	8-methoxypsoralen
ACN	Acetonitrile
BSA	Bovine Serum Albumin
CHCA	$\alpha$ -cyano-4-hydroxycinnamic acid
CMC	Carboxymethylcellulose
DAB	3,3'-diaminobenzidine
DMEM	Dulbecco's Modified Eagle Medium
EMA	European Medicines Agency
FDA	Food and Drug Administration
HBSS	Hank's Buffered Salt Solution
H&E	Hematoxylin and Eosin
ICH	International Conference for Harmonization
IL	Interleukin
LC-MS	Liquid Chromatography - Mass Spectrometry
LLNA	Local Lymph Node Assay
LN	Lymph Node
LOAEL	Lowest Observed Adverse Effect Level
MALDI	Matrix-Assisted Laser Desorption/Ionization
MEC	Molar Extinction Coefficient
MED	Minimal Erythematous Dose
MXF	Moxifloxacin
MSI	Mass Spectrometry Imaging
NOAEL	No Observed Adverse Effect Level
NRU	Neutral Red Uptake
NSAIDs	Non-Steroidal Anti-Inflammatory Drug
OECD	Organisation for Economic Co-operation and Development
PBS	Phosphate Buffered Saline
PIF	Photo-Irritation-Factor
PLA	Proximity Ligation Assay
ROS	Reactive Oxygen Species
SOP	Standard Operating Procedure
SPX	Sparfloxacin
TFA	Trifluoroacetic Acid
TNF	Tumor Necrosis Factor
UPLC	Ultrahigh-Performance Liquid Chromatography
UV	Ultraviolet
VIS	Visible light



# 1. Introduction

Phototoxicity is a relatively common phenomenon and is an adverse effect of some systemic drugs. A large number of pharmaceutical drug substances are known to carry the potential to elicit a phototoxic response (Moore 2002, Ferguson 2002). Reported cases of phototoxic responses may account for 5 to 10 % of recorded cutaneous adverse drug reactions (Selvaag 1997).

Phototoxicity is an acute light-induced skin response to a photoreactive chemical, which may represent like sunburn (dermatitis solaris). Phototoxicity can be elicited by a wide range of pharmaceutical agents like Non-Steroidal Anti-Inflammatory Drug (NSAIDS) and various anti-infective agents like tetracyclines or fluoroquinolones (Allen, 1993; Epstein, 1985; Gould *et al.*, 1995). On the other hand, photoallergy is an immunologically mediated reaction to a chemical initiated by the formation of photoproducts, which may be more similar to an eczematous dermatitis.

As these abnormal reactions seriously limit or exclude the usage of certain drugs, it is essential to identify such liabilities early in development. Therefore, photosafety of drug candidate molecules needs to be evaluated (ICH M3 R2, 2009).

## 1.1. Photosafety evaluation of pharmaceuticals

The need to perform photosafety evaluation as an integral part of pharmaceutical drug development has developed during the last 20 years. Initial, clinically relevant symptoms were only seen late during development or even after marketing of a new drug. In some cases, e.g. the fluoroquinolones class antibiotics, the risk/benefit assessment had to be changed leading to significant limitations (Domagala, 1994). Approximately 10 years later and following the validation of the in vitro 3T3 Neutral Red Uptake Phototoxicity Test (Spielmann H et al., 1998) in the U.S.A as well as in the E.U. guidance documents were issued detailing the expectations of the regulatory authorities (FDA, 2003; EMEA, 2002). More recently, the European position was slightly revised (EMA Q&A document, 2011) and efforts have been initiated to harmonize regulatory requirements internationally (ICH M3 R2, section 14, 2009; ICH S10, 2013).

In general, the following characteristics are evaluated in order to determine if a drug candidate will present a photosafety concern:

- Absorbance of light within the range of natural sunlight (290-700 nm);
- Generation of reactive species following absorption of UV/visible light; and
- Sufficient distribution to light-exposed tissues (e.g., skin, eye).

If these three conditions are not simultaneously met, a compound will not be considered as potentially phototoxic.

### 1.1.1. Photochemical properties

The first step is to consider the absorption of light in the range of 290 to 700 nm. According to the Molar Extinction Coefficient (MEC)-based approach proposed by Henry and co-workers (Henry, Foti and Alsante, 2009), a compound would be considered to absorb sufficiently light if its MEC value is above  $1000 \text{ L} \cdot \text{mol}^{-1} \cdot \text{cm}^{-1}$ .

Although different mechanisms for phototoxicity are known (e.g. formation of photoadducts or cytotoxic photoproducts), it appears that the excitation of molecules by light can typically lead to generation of Reactive Oxygen Species (ROS), including superoxide and singlet oxygen *via* energy transfer mechanisms. Thus, ROS generation following irradiation with UV or visible light can be an indicator of phototoxic potential (Onoue *et al.*, 2010).

### 1.1.2. Tissue Distribution/Pharmacokinetics

A variety of factors influence the ability of a photoreactive chemical to reach light-exposed tissues. The plasma concentration, the perfusion of the tissue, the partitioning from vascular to interstitial and cellular compartments, and the binding, retention, and accumulation will influence concentration of the chemical in the tissue. If a photoreactive chemical reaches light-exposed tissues, a phototoxic reaction might occur depending on the excitation wavelength. UVA and visible light photons sufficiently penetrate into deeper skin layers. In comparison, only a small fraction of UVB reaches the dermis.

Binding, retention or accumulation of a compound in sun-exposed tissue might be taken into consideration as longer residence times or higher tissue to plasma concentration ratios may increase the probability of a phototoxic tissue reaction.

### 1.1.3. Nonclinical photosafety testing

The available and routinely used nonclinical assays, both *in vitro* and *in vivo* (e.g. UV-vis light absorption spectrum, *in vitro* 3T3 Neutral Red Uptake phototoxicity test, oral UV Local Lymph Node Assay), are focused primarily on detecting potential phototoxicity. The most widely used *in vitro* assay for phototoxicity is the *in vitro* 3T3 Neutral Red Uptake Phototoxicity Test (3T3 NRU-PT) as it is considered the most appropriate *in vitro* screen for soluble compounds that are not exclusively UVB absorbers (OECD guideline, 2004). However, this monolayer cell culture assay shows a high frequency of positive results and may overpredict the human photosafety risk (Lynch & Wilcox, 2011).

For both *in vitro* and *in vivo* assays, the selection of irradiation conditions is critical. The broadest range of light exposure that humans might be regularly exposed to is natural sunlight. Therefore it is important to select a suitable sunlight simulator light source. Irradiance and irradiation dose are normalized based on the UVA part (320 to 400 nm) of the applied spectrum. UVA doses ranging from 5 to 20 J/cm<sup>2</sup> have been used to establish *in vitro* and *in vivo* phototoxicity assays as they are comparable to those obtained during outdoor activities on summer days at noon time, in temperate zones, and at sea level (ICH, S10, 2013).

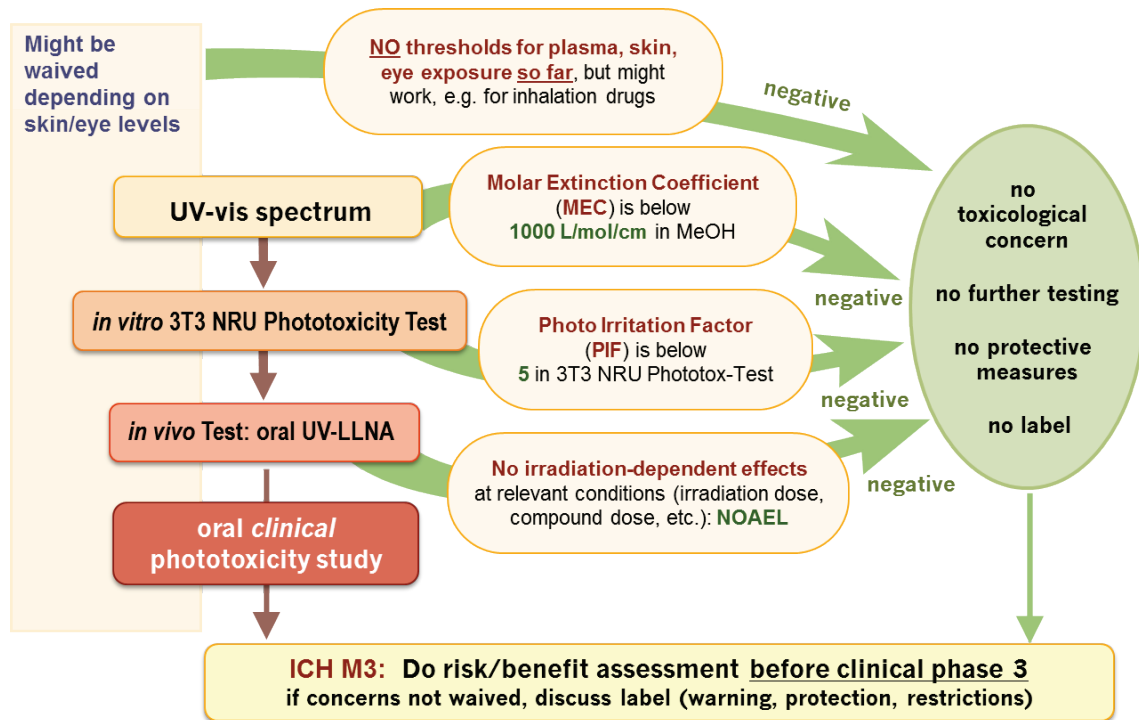


Figure 1. Flowchart representing the staged approach for photosafety assessment currently internally applied in Novartis.

## 1.2. Scope of the thesis

In this work, we were interested in a more in-depth understanding of the underlying mechanisms of phototoxicity, particularly *in vivo*. The results of our investigation of phototoxicity mechanisms are presented in three research papers published in peer reviewed journals which represent the different sections of this thesis.

In the first manuscript (Boudon et al., 2013), we report the further optimization of the establishment of modified murine UV-local lymph node assay (UV-LLNA), adapted for phototoxicity assessment of systemically applied compounds. Several clinically phototoxic reference compounds were tested in mice using a sun light simulator to establish time- and dose-dependent profiles. The reference compounds included sparfloxacin (Dawe et al., 2003; Hamanaka et al., 1998; Lipsky et al., 1999a, 1999b; Pierfitte et al., 2000), enoxacin (Dawe et al., 2003; Izu et al., 1992; Kang et al., 1993), lomefloxacin (Cohen and Bergstresser, 1994; Correia and Delgado, 1994; Man et al., 1999), doxycycline (Bjellerup and Ljunggren, 1994; Blank et al., 1968; Frost et al., 1972; Layton and Cunliffe, 1993), promethazine (Tzanck *et al.*, 1951; Sidi *et al.*, 1955; Epstein and Rowe, 1957; Epstein, 1960; Newill, 1960), vemurafenib (Chapman *et al.*, 2011; Flaherty *et al.*, 2010, Lacouture *et al.* 2013) and ketoprofen (Camarasa, 1985; Alomar, 1985; Foti et al., 2011).

Once time- and dose-dependent profiles of these reference compounds were established, the experimental approach initially included the investigation of co-localization of compound concentration and signs of acute toxicity. The aim was to use immunohistochemical methods to localize and quantify the release of inflammatory markers and the immune cells infiltrate, as well as early developmental stages of inflammation. For this purpose, comprehensive investigations were undertaken with skin samples from the aforementioned *in vivo* studies in

mice. In order to characterize immunocompetent cells, we used antibodies raised against neutrophils, macrophages and lymphocytes. For characterization of secreted markers, we used primary antibodies raised against interleukins IL-1 $\alpha$ , -2, -6, -8, -10, -12 and TNF $\alpha$ . Although promising, this technique is complex and its reliability is not only depending on antibody quality, but also other important factors such as tissue fixation and processing, antigen retrieval and sensitivity of the protein detection system. In order to set up suitable protocols on positive tissues, we used both manual and automatic methods (VENTATA, Roche, Switzerland). We tried different type of sample fixation (Tissues fixed in Formalin during 2 hours or 48 hours, in HISTOCHOICE™ during 6 hours or cryosections with no fixation or fixed with Formaldehyde 4%, Glutaraldehyde or Acetone). Pretreatment of the tissues, antigen retrievals (Protease 1, Borate, Citrate pH6 or pH7) and different type of detection methods (Labeled Streptavidin Biotin revelation with Vector VIP reagent, Avidine Biotin Complex revelation with DAB (3,3'-diaminobenzidine), Avidine Biotin Complex revelation with Alkaline Phosphatase and counterstained with Hematoxylin or 2% methylgreen, and Duolink in situ Proximity Ligation Assay (PLA) method) were also investigated. Unfortunately, the results were not conclusive and are not presented in this work.

In the second manuscript, we focused our work on vemurafenib, a B-Raf kinase inhibitor for the treatment of patients with unresectable or metastatic melanoma carrying the BRAFV600E mutation. It is commercially available since 2011 (Zelboraf, Roche). We selected this drug because signs of clinical photosensitivity were reported in 42 % of patients included in the Phase I trial extension cohort. Similarly, during Phase II and Phase III, 52 % and 30 % of vemurafenib-treated patients were affected, respectively (Chapman *et al.*, 2011; Flaherty *et al.*, 2010, Lacouture *et al.* 2013). Surprisingly, the phototoxic potential evaluation in an

animal model during drug development concluded that there would exist no relevant risk for humans. Therefore, it became a fundamental question to understand this discrepancy.

The aforementioned mouse oral UV-Local Lymph Node Assay, was used to investigate the impact of formulations, dose levels, duration of treatment and timing of irradiation. Moreover a basic pharmacokinetic profile was established within the same mouse strain.

The third manuscript covers investigations on imaging techniques to follow the fate of photoreactive molecules in tissue samples. Matrix-assisted laser desorption/ionization mass spectrometry (MALDI-MS)-based imaging (MSI) was applied to evaluate the distribution of sparfloxacin, an antibiotic drug belonging to the class of fluoroquinolones and a well-known photosensitizer in human. Both, samples from mouse skin and from a human 3D skin model were used in order to assess the potential advantage of this technique in the context of photosafety evaluation.

## References

- Allen, J.E. 1993. Drug-induced photosensitivity. *Clin. Pharm.* **12**: 580–587.
- Alomar, A. 1985. Ketoprofen photodermatitis. *Contact Dermatitis*. **12**(2): 112-3.
- Bjellerup, M., Ljunggren, B. 1994. Differences in phototoxic potency should be considered when tetracyclines are prescribed during summertime: a study on doxycycline and lymecycline in human volunteers, using an objective method for recording erythema. *Br. J. Dermatol.* **130**: 356-360.
- Blank, H., Cullen, S.I., Catalano, P.M. 1968. Photosensitivity studies with demethylchlortetracycline and doxycycline. *Arch. Derm.* **97**: 1-2.

- Boudon, S.M, Plappert-Helbig, U., Odermatt, A., Bauer, D. 2013. Characterization of vemurafenib phototoxicity in a mouse model. *Toxicol. Sci.*, doi: 10.1093/toxsci/kft237, first published online: October 23, 2013.
- Camarasa, J.G. 1985. Contact dermatitis to ketoprofen. *Contact Dermatitis*. **12**(2):120-2.
- Chapman, P.B., Hauschild, A., Robert, C., Haanen, J.B., Ascierto, P., Larkin, J., Dummer, R., Garbe, C., Testori, A., Maio, M., Hogg, D., Lorigan, P., Lebbe, C., Jouary, T., Schadendorf, D., Ribas, A., O'Day, S.J., Sosman, J.A., Kirkwood, J.M., Eggermont, A.M., Dreno, B., Nolop, K., Li, J., Nelson, B., Hou, J., Lee, R.J., Flaherty, K.T., McArthur, G.A. and BRIM-3 Study Group (2011). Improved survival with vemurafenib in melanoma with BRAF V600E mutation. *N. Engl. J. Med.* **364**:2507–2516.
- Cohen, J.B., Bergstresser, P.R. 1994. Inadvertent phototoxicity from home tanning equipment. *Arch. Dermatol.* **130**: 804-806.
- Correia, O., Delgado, L. 1994. Bullous photodermatosis after lomefloxacin. *Arch. Dermatol.* **130**: 808-809.
- Dawe, R.S., Ibbotson, S.H., Sanderson, J.B., Thomson, E.M., Ferguson, J. 2003. A randomized controlled trial (volunteer study) of sitafloxacin, enoxacin, levofloxacin and sparfloxacin phototoxicity. *Br. J. Dermatol.* **149**: 1232-1241.
- Domagala, J.M. 1994. Structure–activity and structure–side-effect relationships for the quinolone antibacterials, *J. Antimicrob. Chemother.* **33**: 685–706.
- EMA Note for Guidance on photosafety testing, EMA, CPMP/SWP/398/01, London, 27 June 2002.
- EMA Questions and answers on the ‘Note for guidance of photosafety testing’, EMA, CHMP/SWP/336670, London, 17 March 2011.
- Epstein, S. 1960. Allergic photocontact dermatitis from promethazine (phenergan). *Arch Dermatol.* **81**:175-80.
- Epstein, S., Rowe, R.J. 1957. Photoallergy and photocross-sensitivity to phenergan. *J Invest Dermatol.* **29**(5):319-26.

- Epstein, J.H., Wintroub, B.U. 1985. Photosensitivity due to drugs. *Drugs* **30**: 42–57.
- FDA Guidance for Industry on Photosafety Testing, US Department of Health and Human Services—  
Food and Drug Administration, Center for Drug Evaluation and Research (CDER), May 2003,  
Pharmacology and Toxicology, Rockville, MD, USA.
- FDA Guidance for Industry on Photosafety Testing, US Department of Health and Human Services—  
Food and Drug Administration, Center for Drug Evaluation and Research (CDER), January 2000,  
Pharmacology and Toxicology, Rockville, MD, USA.
- Ferguson, J. 2002. Photosensitivity due to drugs. *Photodermatol. Photoimmunol. Photomed.*  
**18**(5):262-9.
- Flaherty, K.T., Puzanov, I., Kim, K.B., McArthur, G.A., Sosman, J.A., O'Dwyer, P.J., Lee,  
R.J., Grippo, J.F., Nolop, K. and Chapman, P.B. (2010). Inhibition of mutated, activated BRAF in  
metastatic melanoma. *N. Engl. J. Med.* **363**:809–819.
- Foti, C., Cassano, N., Vena, G.A., Angelini, G. 2011. Photodermatitis caused by oral ketoprofen: two  
case reports. *Contact Dermatitis.* **64**: 181-183.
- Frost, P., Weinstein, G.D., Gomez, E.C. 1972. Phototoxic potential of minocycline and doxycycline.  
*Arch. Derm.* **105**: 681-683.
- Gould, J.W., Mercurino, M.G., Elemets, C.A. 1995. Cutaneous photosensitivity diseases induced by  
exogenous agents. *J. Am. Acad. Dermatol.* **33**(4):551–573.
- Hamanaka, H., Mizutani, H., Shimizu, M. 1998. Sparfloxacin-induced photosensitivity and the  
occurrence of a lichenoid tissue reaction after prolonged exposure. *J. Am. Acad. Dermatol.* **38**:  
945-949.
- Henry, B., Foti, C., Alsante, K. 2009. Can light absorption and photostability data be used to assess  
the photosafety risks in patients for a new drug molecule? *J Photochem Photobiol B.* **96**(1):57-62.
- ICH, M3 (R2). 2009. Guidance on nonclinical safety studies for the conduct of human clinical trials  
and marketing authorization of pharmaceuticals.  
[http://www.ich.org/fileadmin/Public\\_Web\\_Site/ICH\\_Products/Guidelines/Multidisciplinary/M3\\_R2/Step4/M3\\_R2\\_Guideline.pdf](http://www.ich.org/fileadmin/Public_Web_Site/ICH_Products/Guidelines/Multidisciplinary/M3_R2/Step4/M3_R2_Guideline.pdf).

ICH (2012), draft guideline S10 “Photosafety evaluation of pharmaceuticals”,

<[http://www.ich.org/fileadmin/Public\\_Web\\_Site/ICH\\_Products/Guidelines/Safety/S10/S10\\_Step\\_2.pdf](http://www.ich.org/fileadmin/Public_Web_Site/ICH_Products/Guidelines/Safety/S10/S10_Step_2.pdf)>.

Izu, R., Gardeazabal, J., González, M., Landa, N., Ratón, J.A., Díaz-Pérez, J.L. 1992. Enoxacin-induced photosensitivity: study of two cases. *Photodermatol. Photoimmunol. Photomed.* **9**: 86-88.

Kang, J.S., Kim, T.H., Park, K.B., Chung, B.H., Youn, J.I. 1993. Enoxacin photosensitivity. *Photodermatol. Photoimmunol. Photomed.* **9**: 159-161.

Lacouture, M.E., Duvic, M., Hauschild, A., Prieto, V.G., Robert, C., Schadendorf, D., Kim, C.C., McCormack, C.J., Myskowski, P.L., Spleiss, O., Trunzer, K., Su, F., Nelson, B., Nolop, K.B., Grippo, J.F., Lee, R.J., Klimek, M.J., Troy, J.L., Joe, A.K. (2013). Analysis of dermatologic events in vemurafenib-treated patients with melanoma. *Oncologist.* **18**(3):314-22.

Layton, A.M., Cunliffe, W.J. 1993. Phototoxic eruptions due to doxycycline – a dose-related phenomenon. *Clin. Exp. Dermatol.* **18**: 425-427.

Lipsky, B.A., Dorr, M.B., Magner, D.J., Talbot, G.H., 1999a. Safety profile of sparfloxacin, a new fluoroquinolone antibiotic. *Clin. Ther.* **21**: 148-159.

Lipsky, B.A., Miller, B., Schwartz, R., Henry, D.C., Nolan, T., McCabe, A., Magner, D.J., Talbot, G.H., 1999b. Sparfloxacin versus ciprofloxacin for the treatment of community-acquired, complicated skin and skin-structure infections. *Clin. Ther.* **21**: 675-690.

Lynch A.M., Wilcox P. 2011. Review of the performance of the 3T3 NRU in vitro phototoxicity assay in the pharmaceutical industry. *Exp Toxicol Pathol.* **63**(3):209-14.

Man, I., Murphy, J., Ferguson, J. 1999. Fluoroquinolone phototoxicity: a comparison of moxifloxacin and lomefloxacin in normal volunteers. *J. Antimicrob. Chemother.* **43** (Suppl. B): 77-82.

Moore, E.M. 2002. Drug-induced cutaneous photosensitivity. *Drug Saf.* **25**: 345-372.

Newill, R.G. 1960. Photosensitivity caused by promethazine. *Br Med J.* **2**(5195):359-60.

OECD Guidelines for the Testing of Chemicals Section 4. 2004. Test No. 432: In vitro 3T3 NRU phototoxicity test.

- Onoue, S., Kawamura, K., Igarashi, N., Zhou, Y., Fujikawa, M., Yamada, H., Tsuda, Y., Seto, Y., Yamada, S. 2008. Reactive oxygen species assay-based risk assessment of drug-induced phototoxicity: classification criteria and application to drug candidates. *Pharm Biomed Anal.* **47**(4-5):967-72.
- Pierfitte, C., Royer, R.J., Moore, N., Bégaud, B. 2000. The link between sunshine and phototoxicity of sparfloxacin. *Br. J. Clin. Pharmacol.* **49**: 609-612.
- Selvaag, E. 1997. Clinical drug photosensitivity – A retrospective analysis of reports to the Norwegian Adverse Drug Reactions Committee from the years 1970-1994. *Photodermatol. Photoimmunol. Photomed.* **13**: 21-23
- Spielmann, H., Balls, M., Dupuis, J., Pape, W.J., Pechovitch, G., de Silva, O., Holzhütter, H.G., Clothier, R., Desolle, P., Gerberick, F., Liebsch, M., Lovell, W.W., Maurer, T., Pfannenbecker, U., Potthast, J.M., Csato, M., Sladowski, D., Steiling, W., Brantom, P. 1998. The International EU/COLIPA In Vitro Phototoxicity Validation Study: Results of Phase II (Blind Trial). Part 1: The 3T3 NRU Phototoxicity Test. *Toxicol In Vitro.* **12**(3):305-27.
- Sidi, E., Hincky, M., Gervais, A. 1955. Allergic sensitization and photosensitization to phenergan cream. *J Invest Dermatol.* **24**(3):345-52.
- Toback A.C., Anders J.E. 1986. Phototoxicity from systemic agents. *Dermatol. Clin.* **4**(2):223-230.
- Tzanck, Sidi, Mazalton, Kohen. 1951. Two cases of dermatitis from phenergan with photosensitization. *Bull Soc Fr Dermatol Syphiligr.* **58**(4):433.

## 2. Integrated preclinical photosafety testing strategy for systemically applied pharmaceuticals

[Schümann, J., Boudon, S. M., Ulrich, P., Loll, N., Garcia, D., Schaffner, R., Streich, J., Kittel, B., and Bauer, D. 2013. Integrated preclinical photosafety testing strategy for systemically applied pharmaceuticals. *Toxicological Sciences*.] Submitted

**This work was presented at the EUROTOX 2013. Interlaken, Switzerland, Sept. 2013.**

Boudon, S., Schneider, M., Morandy, G., Junker, U., Plappert-Helbig, U., Odermatt, A., Bauer, D. A modified oral UV-LLNA in Balb/c mice to investigate phototoxicity mechanisms and pharmacokinetic properties in skin. *Toxicology Letters*. Volume 221. Supplement. 28 August 2013, Pages S87-S88, ISSN 0378-4274.

<http://dx.doi.org/10.1016/j.toxlet.2013.05.107>.

## Abstract

Phototoxic properties of systemically applied pharmaceuticals may be the cause of serious adverse drug reactions. Therefore, a reliable preclinical photosafety assessment strategy, combining *in vitro* and *in vivo* approaches in a quantitative manner is important and has not been described so far. Here we report the establishment of an optimized modified murine local lymph node assay (LLNA), adapted for phototoxicity assessment of systemically applied compounds, as well as the test results for 34 drug candidates in this *in vivo* photo-LLNA. The drug candidates were selected based on their ability to absorb ultraviolet/visible light and the photo irritation factors (PIF) determined in the well-established *in vitro* 3T3 neutral red uptake phototoxicity test. An *in vivo* phototoxic potential was identified for 13 of these drug candidates. The use of multiple dose levels in the described murine *in vivo* phototoxicity studies enabled the establishment of no- and/or lowest-observed-adverse-effect-levels (NOAEL/LOAEL), supporting also human photosafety assessment. An *in vitro* – *in vivo* correlation demonstrated that a drug candidate classified as “phototoxic” *in vitro* is not necessarily phototoxic *in vivo*. However, the probability for a drug candidate to cause phototoxicity *in vivo* clearly correlated with the magnitude of the phototoxicity identified *in vitro*.

## 2.1. Introduction

Phototoxicity of pharmaceutical products may cause serious adverse drug reactions. This does not only apply to topically applied chemicals absorbing ultraviolet (UV) and/or visible (vis) light, but also to those which reach light-exposed tissues such as skin or eyes following systemic exposure (for review see Drucker and Rosen, 2011; Ferguson, 2002; Moore, 2002). The contact phototoxic potential of topically applied pharmaceuticals is typically assessed preclinically using *in vivo* phototoxicity assays. These include monitoring of skin reactions in topically treated guinea pigs or the murine local lymph node assay (LLNA) in albino mice, including its non-radioactive modifications (for these, the term “modified LLNA” is commonly used), with quantification of skin and lymph node (LN) reactions (Homey et al., 1998; Neumann et al., 2005; Ulrich et al., 2001; Vohr et al., 2001). However, for systemically applied pharmaceuticals, an integrated preclinical photosafety assessment strategy has not been established so far.

The standard preclinical *in vitro* assay for phototoxicity assessment is the “*in vitro* 3T3 neutral red uptake (NRU) phototoxicity test” (OECD, 2004), which may be considered for compounds showing relevant light absorption in the range of natural sun light (290 to 700 nm) (Bauer et al., 2013). Neumann et al. (2005) and Vohr et al. (2001) reported the testing of selected systemically applied reference compounds in different preclinical *in vitro* and/or *in vivo* assays, including an “integrated model for the differentiation of skin reactions” (IMDS) based on a modified murine LLNA with endpoints limited to ear thickness, local lymph node (LN) weight and cell counts.

Here we report the establishment of a further optimized and extended modified murine LLNA, adapted for phototoxicity assessment of systemically applied compounds (photo-LLNA), the correlation between the *in vitro* and *in vivo* photosafety testing of 34 drug candidates in this system, and the relevance to preclinical photosafety assessment. The reference compounds included sparfloxacin (Dawe et al., 2003; Hamanaka et al., 1998; Lipsky et al., 1999a, 1999b; Pierfitte et al., 2000), enoxacin (Dawe et al., 2003; Izu et al., 1992; Kang et al., 1993), lomefloxacin (Cohen and Bergstresser, 1994; Correia and Delgado, 1994; Man et al., 1999), doxycycline (Bjellerup and Ljunggren, 1994; Blank et al., 1968; Frost et al., 1972; Layton and Cunliffe, 1993), ketoprofen (Bagheri et al., 2000; Foti et al., 2011), and 8-methoxypsoralen (8-MOP), the latter also being used as an orally administered photoactive drug together with UVA irradiation in photochemotherapy (“PUVA”, psoralen + UVA) of severe psoriasis (for review see Lapolla et al., 2011). For completeness, previously reported results with the reference compound vemurafenib (Boudon et al., 2013) are included as well.

In addition to clinically relevant reference compounds, 34 systemically applied drug candidates were tested at three dose levels in this *in vivo* assay. The following major optimizations compared to the described IMDS for systemically applied phototoxic reference compounds (Neumann et al., 2005; Vohr et al., 2001) were done: *i.* systematic monitoring of erythema formation at least twice daily using a defined scoring system, *ii.* determination of ear biopsy weights instead of ear thickness, *i.e.* exclusion of a subjective component associated with the measurement of ear thickness using a micrometer (Ulrich and Vohr, 2012), *iii.* inclusion of histopathological analysis of the retina due to residual absorption of visible light at wavelengths that reach the human retina. Altogether, determination

of erythema formation and ear weight, local LN reactions (quantification of LN weights and cell counts), and retina changes as well as identification of a no- or lowest-observed-adverse-effect-level (NOAEL/LOAEL) are described as key elements supporting later human photosafety assessment. Finally, the implications of an *in vitro* – *in vivo* phototoxicity correlation on the preclinical *in vivo* photosafety testing strategy are discussed.

## 2.2. Materials and Methods

### 2.2.1. UV/visible light absorption spectra

Light absorption spectra within sun light range (290 to 700 nm) were recorded on a Cary 300 spectrophotometer (Varian Australia Pty Ltd, Australia) using UV-transparent quartz glass cuvettes (1 cm path length). Substances were dissolved in methanol applying individual solvent-specific baseline correction. For each peak (and for 290 nm if this was the highest observed absorption value) the molar extinction coefficient ( $\epsilon$  or MEC) was calculated:  $\epsilon = A / (c \times l)$  (**A**, absorbance; **c**, concentration; **l**, path length (cuvette)).

### 2.2.2. In vitro 3T3 NRU phototoxicity test

The BALB/c mouse fibroblast cell line 3T3.A31 was obtained from the European Collection of Cell Cultures (ECACC, no. 86110401, at passage 82), United Kingdom. Cells were cultivated in Dulbecco's Modified Eagle Medium (DMEM) (with phenol red) containing 10% fetal calf serum, 1% glutamine, and 1%

penicillin/streptomycin. The assay was performed in accordance with OECD Testing Guideline 432. Briefly, 24 hours after seeding the mouse fibroblast cells (not exceeding passage 99) into 96-well plates, the medium was removed and the cells were treated with different concentrations of the test compound for 1 hour using Hank's Balanced Salt Solution (HBSS, without phenol red) as medium replacement. Subsequently, these cells were irradiated (+Irr) with simulated sun light (SOL500 H1, Dr. Hönle, Germany) with a main spectral output from 320 until beyond 700 nm. The integrated H1 filter system attenuated the highly cytotoxic UVB range to a level which was tolerated by the cell culture as suggested by the mentioned guideline. In parallel, an identically prepared 96-well plate was kept in the dark (-Irr), serving as control. UVA irradiance was measured by a UVA meter (Dr. Hönle, Germany) with spectral sensitivity in the range from 320 to 400 nm and a measuring range between 0 and 199.9 mW/cm<sup>2</sup>. The yearly calibration using an externally calibrated spectroradiometer covering the full spectral range from 250 to 800 nm was performed by opto.cal GmbH (Switzerland), which is a calibration laboratory accredited by the Swiss Accreditation Service. The applied intensity was 1.67 mW/cm<sup>2</sup> resulting in a total UVA dose of 5 J/cm<sup>2</sup> after 50 minutes of irradiation. After irradiation the HBSS buffer was replaced by fresh medium. Cell viability was determined 24 hours later using neutral red as the vital dye, which was measured at 540 nm after incubation and extraction. The PIF was calculated according to OECD TG 432 using the following equation:  $PIF = IC_{50}(-Irr) / IC_{50}(+Irr)$ .

### 2.2.3. Mice

Female BALB/c mice, obtained in a specific pathogen-free state from Charles River Laboratories (France or Germany), were used throughout the studies, usually at the age of 8 to 10 weeks. The photo-LLNA studies were performed in conformity with the Swiss Animal Welfare Law and in accordance with internal standard operating procedures and guidelines for care and use of laboratory animals. Mice had *ad libitum* access to pelleted standard rodent diet and tap water from the domestic supply and were kept under temperature- and humidity-controlled conditions and an automatic 12 hour light/dark cycle with background radio coordinated with light hours.

### 2.2.4. Treatment of mice

For the establishment of the optimized modified murine systemic photo-LLNA the following reference compounds (all obtained from Sigma-Aldrich, Switzerland, with the exception of 8-MOP, for which meladine tablets from Galderma, Switzerland, were used) were administered by oral gavage at three dose levels (twelve mice per group) once a day for three consecutive days: sparfloxacin (in 1% (w/v) aqueous solution of carboxymethylcellulose (CMC)); enoxacin (in water); doxycycline (in water); ketoprofen (in 0.5% CMC). Lomefloxacin (in water) was used as reference compound at three dose levels but only administered for two consecutive days, and meladine (in water) was administered at two dose levels only for three consecutive days. Drug candidates were administered systemically (by oral gavage or intravenously) at three dose

levels in suitable vehicles for three consecutive days. Selection of dose levels was mostly based on expected maximal tolerated exposure (high dose level), pharmacologically relevant exposure (low dose level), and an exposure level in between those two (intermediate dose level).

### 2.2.5. Exposure of mice to simulated sun light

During irradiation mice were kept in specific cages allowing only for lateral movements and ensuring a uniform irradiation of their backs and ears. Non-irradiated animals were kept in their housing cages under standard room light. Six mice per dose level were exposed to simulated sun light (Psorisan 900 H1 lamp; Dr. Hönle, Germany) with a main spectral output from 320 until beyond 590 nm. Irradiation was normalized to a dose of 10 J/cm<sup>2</sup> UVA. The integrated H1 filter system attenuated the highly cytotoxic UVB range to a level which was tolerated by the animals. This adjustment is recommended for testing oral drugs, since in such cases photosafety assessment is mainly focusing on UVA and visible light as only these wavelengths are penetrating sufficiently into skin (ICH S10, 2013). With the sun light simulator used, spectral output between 450 and 490 nm and beyond 590 nm was under-represented compared to sun light. However, none of the administered compounds had its absorption peak in these ranges. UVA irradiance was measured with a UV radiometer (Gigahertz-Optik GmbH, Germany). The yearly calibration of this GLP-compliant equipment with an externally calibrated spectroradiometer covering the full spectral range from 250 to 800 nm was performed by opto.cal GmbH (Switzerland). Dose groups were exposed to simulated sun light separately from each other. Selection of the time

point of exposure to simulated sun light was mostly based on pharmacokinetic properties of the compounds (*i.e.* expected  $t_{\max}$ ). Corresponding control groups treated with vehicle, not exposed to simulated sun light, were included. For the reference compounds exposure to simulated sun light started not later than 1.5 hours after treatment (exception: 2 hours for doxycycline).

### 2.2.6. Erythema scoring

During the dosing period, formation of ear skin erythema was monitored at least twice daily using a defined scoring system (0 = no erythema; 1 = slight erythema; 2 = moderate erythema; 3 = strong erythema).

### 2.2.7. Determination of ear biopsy weights and auricular LN weights and cell counts

Approximately 24 hours after the last treatment, mice were sacrificed by exposure to carbon dioxide. If not indicated differently in the results part, from both ears circular pieces from the apical area of each ear with a diameter of 8 mm (= 0.5 cm<sup>2</sup>) were excised using a disposable punch and weighed as pairs on an analytical balance. For assessment of auricular LN weights and cell counts, the superficial parotid LNs that can be found as single LNs at the jugular bifurcation and that are referred to as “auricular LNs” (*c.f.* Van den Broeck et al., 2006; NIH, 1999) here, were excised bilaterally, weighed on an analytical balance and kept in 1 mL ice-cold 0.5% BSA/PBS per pair. LN cell suspensions were prepared by mechanical disruption of the LNs using a stainless steel mesh. From the resulting

suspensions, cell counts were determined in a conductometer (CASY<sup>®</sup> TTC, Schärfe System, Germany).

### 2.2.8. Histopathology of retina

In murine photo-LLNA studies for sparfloxacin and several drug candidates, one eye from each animal was taken and fixed in Davidson's solution. Tissue was embedded in Paraplast<sup>®</sup>, sectioned, stained with hematoxylin and eosin, and examined microscopically. For the human retina only exposure to visible light is relevant, since wavelengths below 400 nm do not sufficiently penetrate human cornea, lens and vitreous body (Dillon et al., 2000; Sliney, 2002; Lei and Yao, 2006; ICH S10, 2013). Therefore, histopathological examination of the retina was not done for all compounds.

### 2.2.9. Statistical analysis

For statistical calculations either SigmaStat or SAS<sup>®</sup> was used. A One-Way-Analysis-of-Variance was used as statistical method. A normality test was performed to assure that the data were normally distributed (significance level = 0.01). The equal variance test was used to check the assumption that the sample was drawn from populations with the same variance (significance level = 0.01). In case of significant results of the One-Way-ANOVA ( $P < 0.05$ ), multiple comparisons were performed with the Student-Newman-Keuls test. If the normality test and/or the equal variance test gave  $P$  values  $< 0.01$ , a suitable transformation (log, square root) was applied; if the normality test and/or equal

variance test still gave P values  $< 0.01$ , the non-parametric Kruskal-Wallis test was used, and in case of a significant result of the Kruskal-Wallis test ( $P < 0.05$ ), multiple comparisons were performed with the Student-Newman-Keuls test for the ranks of the original observations. For the Student-Newman-Keuls test, the confidence level for the difference of the means was set to 95% ( $\alpha = 0.05$ ). Groups of mice treated with compound were statistically compared with the group of mice treated with vehicle and not exposed to simulated sun light. Furthermore, groups of mice treated with compound and exposed to simulated sunlight were compared to corresponding groups not exposed to simulated sun light.

## 2.3. Results

### 2.3.1. Clinically phototoxic reference compounds in the modified murine oral (gavage) photo-LLNA

The UV-vis absorption spectra of six clinically relevant phototoxic compounds, *i.e.* sparfloxacin, enoxacin, lomefloxacin, doxycycline, ketoprofen, and 8-MOP, were recorded and analyzed to identify absorption peaks with associated MECs (**Table 1**). The *in vitro* phototoxic potential of these compounds was identified by determination of PIF values using the well-established 3T3 NRU test. All six reference compounds were phototoxic *in vitro* with PIF values  $> 25$ , and they showed a phototoxic potential in the herein described optimized modified murine oral (gavage) photo-LLNA (**Table 1**). For completeness, the results with the previously reported reference compound vemurafenib (Boudon et al., 2013) are listed as well. Signs of ear skin irritation (erythema and/or increased ear biopsy

Table 1: Combined UV-vis, *in vitro* and *in vivo* data for systemically applied phototoxic drugs (reference compounds, in order of increasing PIF values)

Drug	UV/vis absorption <sup>a</sup>		<i>in vitro</i> 3T3 NRU phototoxicity test <sup>b</sup>		<i>in vivo</i> modified murine photo-LLNA			
	Peak (nm)	MEC (L mol <sup>-1</sup> cm <sup>-1</sup> )	IC <sub>50</sub> -irr (µg/mL)	IC <sub>50</sub> +irr (µg/mL)	PIF	NOAEL/LOAEL <sup>c</sup> (mg/kg body weight)	Skin <sup>d</sup>	Lymph nodes <sup>e</sup>
Enoxacin	345	18300	1000	39	> 26	400 / 800 / 1600	ET n.r.	LW ↑ ≥ 800
Lomefloxacin	290 319	35900 15200	2352	84	28	200 / 400 / 800	ET n.r.	LW ↑ ≥ 200
Vemurafenib	305	22800	1.50	0.052	> 29	100 / 350 / 450 800	ET ≥ 350 (EW ↑ = 350) <sup>f</sup>	LC ↑ ≥ 800
Sparfloxacin	305 375	33600 9800	500	6.2	> 82	25 / 100 / 400	ET ≥ 100	LW ↑ ≥ 100
Ketoprofen	290	2200	1000	4.1	> 240	100 / 200 / 300 (400 / 500) <sup>g</sup>	ET = 500) <sup>g</sup>	LC ↑ ≥ 25
Doxycycline	352	17300	1000	2.3	> 440	100 / 250 / 400	ET ≥ 250	LW ↑ ≥ 250
8-MOP	299	10700	100	0.22	> 457	10 / 20	ET n.r.	LW ↑ = 20
							EW ↑ = 20	LC ↑ = 20

Abbreviations: **MEC**, molar extinction coefficient; **PIF**, photoirritation factor; **NOAEL**, no-observed-adverse-effect-level with regard to phototoxicity; **LOAEL**, lowest-observed-adverse-effect level with regard to phototoxicity; **ET**, erythema; **EW**, ear biopsy weight; **LW**, auricular lymph node weight; **LC**, auricular lymph node cell count; -, no finding with regard to irradiation-dependent effects; **n.r.**, not recorded.

- <sup>a</sup> Numbers in *italics* represent measurements at the lower spectrum cut-off at 290 nm (not at a peak).
- <sup>b</sup> The IC<sub>50</sub> values for cytotoxicity in the absence (-irr) and presence (+irr) of irradiation with simulated sunlight are given in this table. Numbers in *italics* represent the highest tested concentration (not IC<sub>50</sub> values), which was limited by solubility or the maximal assay range (1000 µg/mL), thus preventing the determination of exact PIF values (indicated by PIF “larger than”).
- <sup>c</sup> Three dose levels (exception: 8-MOP, two dose levels) were tested and are given in this table; the NOAEL is underlined; the LOAEL is **bolded**
- <sup>d</sup> Ear skin erythema (ET) and weight (EW) changes are described (with dose levels of occurrence in mg/kg); in the cases of enoxacin lomefloxacin and 8-MOP erythema formation has not been recorded (n.r.) and ear weight changes are based on one ear (instead of pairs of ears).
- <sup>e</sup> Lymph node weight (LW) and cell count (LC) changes are described (with dose levels of occurrence in mg/kg).
- <sup>f</sup> Ear weight increase was observed 1 to 6 hours after irradiation, but decreased to baseline already at 24 hours (Boudon et al., 2013); this additional investigation was not performed at dose levels above 350 mg/kg (LOAEL).
- <sup>g</sup> During dose finding, a limited number of mice (n = 2) was also treated with 400 and 500 mg/kg/day ketoprofen for 2 days only; these dose levels were toxic; erythema formation was observed at 500 mg/kg confirming the phototoxic properties of ketoprofen *in vivo*.

weights) and auricular LN response (increased LN weight and cell count) mostly occurred concomitantly. As an exception, ketoprofen did not induce skin irritation or auricular LN response up to 300 mg/kg/day.

However, during a dose-finding phase, a limited number of mice (n = 2) was also treated with 400 and 500 mg/kg/day ketoprofen. These dose levels were identified to be toxic, but irradiation-dependent erythema formation was observed at 500 mg/kg/day. Hence, the phototoxic properties of ketoprofen were confirmed in BALB/C mice. For all six tested reference compounds, *in vivo* phototoxicity was dose-dependent.

As shown as an example in **Figure 1**, sparfloxacin induced weak signs of irradiation-dependent ear skin irritation (increase of ear biopsy weights) and a LN response (increase of auricular LN cell counts) in the modified murine photo-LLNA at 25 mg/kg/day, establishing the lowest-observed-adverse-effect-level (LOAEL) with regard to phototoxicity. At 100 and 150 mg/kg/day sparfloxacin, all quantitatively determined parameters (ear biopsy weight, auricular LN weight and cell count) were dose-dependently and statistically significantly increased depending on additional exposure to simulated sun light. Due to the robust response, 100 mg/kg/day sparfloxacin was chosen as standard positive control item in further studies using the modified murine photo-LLNA for systemically applied drug candidates. The mean values and standard deviations of sparfloxacin/irradiation-induced ear biopsy weight as well as auricular LN weight and cell count changes derived from 21 studies, in which sparfloxacin was used as the positive control item, are described in **Table 2**. On average, ear biopsy weights increased by a factor of 1.58, auricular LN weights by a factor of 1.77, and auricular LN cell counts by a factor of 2.18, depending on additional exposure

to simulated sun light. 100 mg/kg/day sparfloxacin, which absorbs visible light relevant for the human retina (Boudon et al., 2013), also induced irradiation-dependent pathological alterations in the retina.

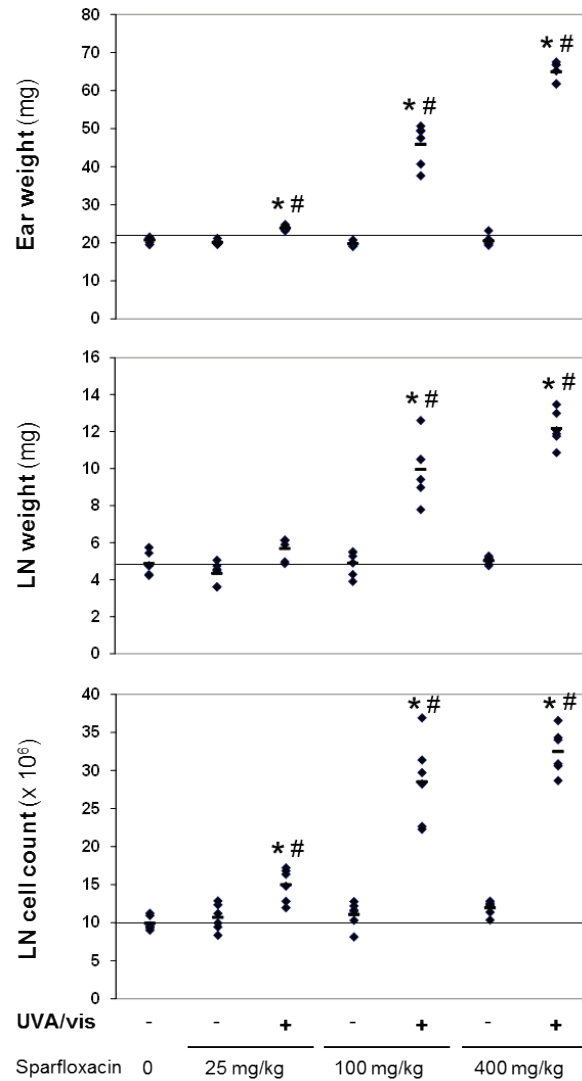


Figure 1: Irradiation-dependent increase of ear weight and auricular LN weight and cell count following oral (gavage) administration of sparfloxacin to female BALB/c mice in the modified murine photo-LLNA. \*  $P < 0.05$  vs vehicle control; #  $P < 0.05$  vs corresponding non-irradiated group.

Sparfloxacin (100 mg/kg)	Ear weight (mg)		LN weight (mg)		LN cell count (x 10 <sup>6</sup> )	
	-	+	-	+	-	+
<b>Irradiation (UVA/vis)</b>	-	+	-	+	-	+
<b>Mean ± SD</b>	20.6 ± 0.9	32.5 ± 6.8	4.7 ± 0.9	8.3 ± 1.7	9.6 ± 2.6	20.9 ± 6.9

Table 2: Ear weight and LN weight and cell count results (mean ± SD) from 21 photo-LLNA studies, in which 100 mg/kg sparfloxacin was used as positive control

As shown in **Figure 2**, sparfloxacin induced irradiation-dependent minimal to moderate atrophy and degeneration in the retina. Reduced thickness, disorganized appearance of the outer nuclear layer and loss of nuclei from rods and cones were the most prominent features. Although less prominent, changes were also present in the inner nuclear layer, *e.g.* loss of cytoplasmic detail in the outer limiting membrane, inner and outer segments of rods and cones up to almost complete loss of these structures in more pronounced cases. In addition, minimal to slight hypertrophy was present in the retinal pigment epithelium. The observed changes were generally consistent with those reported after toxic retinal injury. Finally, 100 and 400 (but not 25) mg/kg/day sparfloxacin induced moderate erythema formation within five to six hours after the first treatment depending on additional exposure to simulated sun light (**Figure 3A**). Over the following two days, a dose-dependent increase in the severity and persistence of erythema was noted. A similar phenomenon was also observed with doxycycline and ketoprofen.

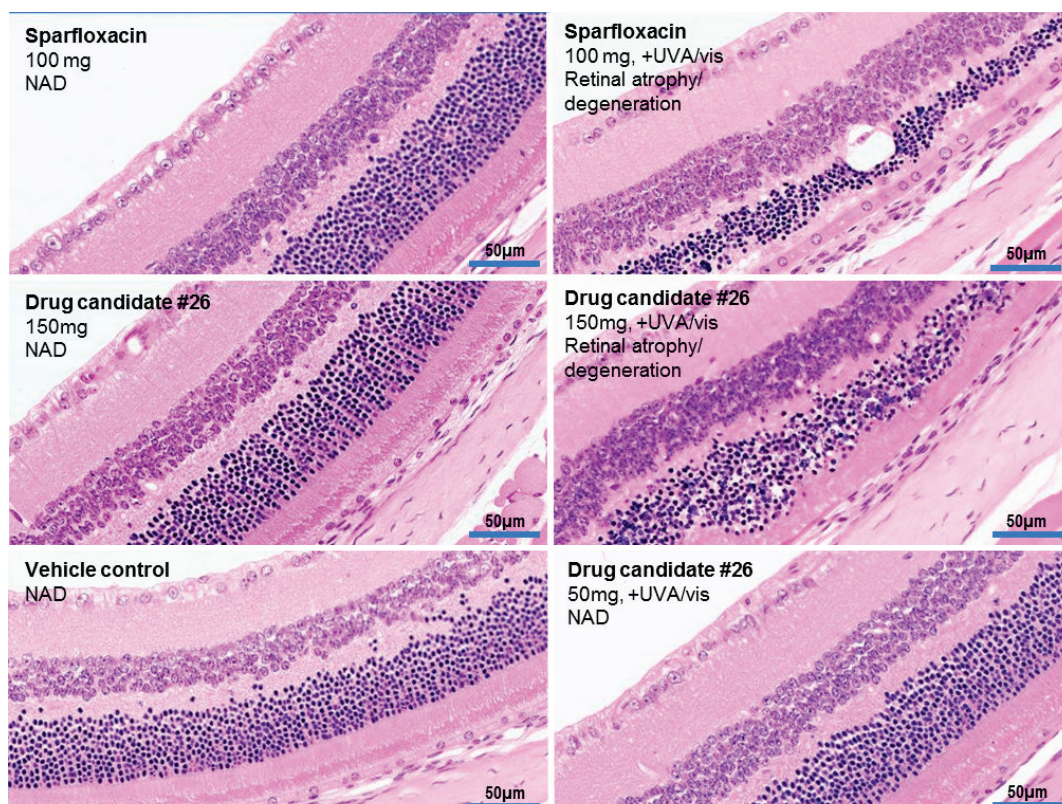


Figure 2: Irradiation-dependent retina changes (retinal atrophy/degeneration) following oral administration of sparfloxacin or drug candidate # 26 to female BALB/c mice in the modified murine photo-LLNA. NAD = no abnormality detected

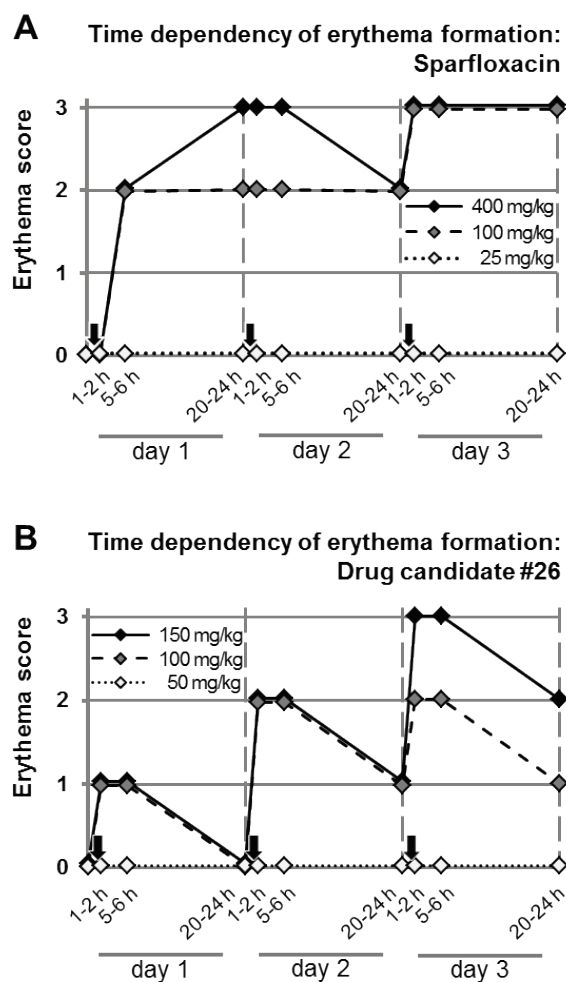


Figure 3: Time- and irradiation-dependent erythema formation (ear skin) following oral (gavage) administration of sparfloxacin (A) or drug candidate #26 (B) to female BALB/c mice in the modified murine photo-LLNA. Arrows indicate treatment/irradiation.

### 2.3.2. Drug candidates in the modified murine systemic photo-LLNA

The UV-vis absorption spectra of 34 systemically applied drug candidates were recorded and analyzed to identify absorption peaks with associated molar extinction coefficients (MEC) and to assess the need and relevance of retina evaluation due to residual absorption of visible light, which is relevant for the human retina (**Table 3**). The phototoxic potential of these drug candidates was determined *in vitro* with the 3T3 NRU test and *in vivo* with the optimized modified murine photo-LLNA. Out of the 34 drug candidates, three had a PIF < 2 (“not phototoxic”), three had a PIF between 2 and 5 (“probably phototoxic”), and 28 had a PIF > 5 (“phototoxic”). As shown in **Table 3**, all 17 drug candidates with a PIF up to at least 33 did not show a phototoxic potential in the *in vivo* assay. Furthermore, the probability for a drug candidate to cause phototoxicity *in vivo* correlated with the magnitude of the phototoxicity identified *in vitro*. 76 % of all tested drug candidates with a PIF  $\geq 36$  and 92% of all drug candidates with a PIF  $\geq 56$  showed a phototoxic potential in the *in vivo* assay. **Figure 4A** shows the frequencies of compounds identified as phototoxic *in vivo* relative to *in vitro* PIF (categorized). **Figure 4B** shows the categorized distribution of PIF values (histogram, n = 100), derived from a historical database of an unbiased selection of drug candidates covering approximately three years.

Table 3: Combined UV-vis, *in vitro* and *in vivo* data for 34 systemically applied drug candidates (“drug”, in order of increasing PIF values)

Drug	UV/vis absorption <sup>a</sup>		<i>in vitro</i> 3T3 NRU phototoxicity test <sup>b</sup>			<i>in vivo</i> modified murine photo-LLNA			
	Peak (nm)	MEC (L·mol <sup>-1</sup> ·cm <sup>-1</sup> )	IC <sub>50</sub> -irr (µg/mL)	IC <sub>50</sub> +irr (µg/mL)	PIF	NOAEL/LOAEL <sup>c</sup> (mg/kg body weight)	Skin <sup>d</sup>	Lymph nodes <sup>e</sup>	Retina atrophy <sup>f</sup>
1	314	23900	3.5	2.9	<b>1.2</b>	10 / 100 / <u>200</u>	-	-	-
2	315	3200	592	414	<b>1.4</b>	30 / <u>100</u> <sup>g</sup>	-	-	-
3	313	14460	304	209	<b>1.5</b>	3 / 30 / <u>100</u>	-	-	-
4	328	20070	40.0	15.7	> <b>2.5</b>	10 / 30 / <u>100</u>	-	-	-
5	290	8290	56.3	16.7	<b>3.4</b>	10 / 30 / <u>75</u>	-	-	-
6	290 317	16790 16240	10.7	3.1	<b>3.4</b>	5 / 15 / <u>50</u>	-	- <sup>h</sup>	-
7	299 356	17700 21440	216	35.5	> <b>6.1</b>	100 / 300 / <u>1000</u>	-	-	-
8	324	4420	1000	135	> <b>7.4</b>	30 / 200 / <u>600</u>	-	-	-
9	290	29240	59.2	6.2	<b>9.6</b>	50 / 150 / <u>400</u>	-	-	-
10	297	12600	10.3	0.73	<b>14</b>	3 / 10 / <u>30</u>	-	-	-
11	311	40800	10	0.64	> <b>16</b>	500 / 1000 / 2000	-	-	-
12	440	12240	12.2	0.69	<b>17</b>	25 / 100 / <u>400</u>	-	-	-
13	434	12800	9.8	0.56	<b>18</b>	50 / 250 / <u>750</u>	-	-	not done
14	290	30620	47.7	2.3	<b>21</b>	10 / 50 / <u>100</u>	-	- <sup>h</sup>	-
15	303	13800	38.9	1.8	> <b>21</b>	10 / 100 / <u>1000</u>	-	-	not done
16	302	31100	13.5	0.45	> <b>30</b>	100 / 500 / <u>2000</u>	-	-	not done
17	290	23670	1.9	0.058	> <b>33</b>	1 / 3 / <u>10</u>	-	-	not done
18	314	4600	1000	28.2	> <b>36</b>	125 / 250 / <u>500</u>	-	-	not done
19	290	12700	104	2.9	<b>36</b>	10 / <u>30</u> / <b>100</b>	ET -	LW ↑ = 100 EW ↑ = 100 LC ↑ = 100	not done
20	325	49280	10.0	0.22	> <b>46</b>	<u>10</u> / <b>50</b> / 150	ET ≥ 50 EW ↑ = 150	LW ↑ = 150 LC ↑ = 150	1/6 at 50 2/6 at 150
21	290 321	18340 8930	6.6	0.14	<b>48</b>	5 / 10 / <u>20</u>	-	- <sup>h</sup>	-

Integrated preclinical photosafety testing strategy for  
systemically applied pharmaceutical | 33

22	<b>373</b>	<b>6750</b>	<b>259</b>	<b>4.9</b>	> 53	<b>25 / 75 / <u>200</u></b>	-	-	-
23	309 328	30090 30550	<i>10.0</i>	0.18	> <b>56</b>	<i>10 / 30 / 100<sup>i</sup></i> <i><u>500 / 1000 / 2000</u></i>	ET ≥ 1000 EW ↑ ≥ 1000	LW ↑ = 2000 LC ↑ = 2000	-
24	320 356	12930 15380	<b>36.8</b>	0.39	> <b>94</b>	<u>50 / 125 / 250</u>	ET ≥ 125 EW ↑ ≥ 125	LW ↑ ≥ 125 LC ↑ ≥ 125	not done
25	308 354	13100 15490	50.4	0.40	<b>125</b>	<b>100 / 300<sup>g</sup></b>	ET ≥ 100 EW ↑ ≥ 100	LW ↑ ≥ 100 LC ↑ ≥ 100	not done
26	301 344	14890 9440	4.8	0.033	<b>146</b>	<u>50 / 100 / 150</u>	ET ≥ 100 EW ↑ ≥ 100	LW ↑ ≥ 100 LC ↑ ≥ 100	4/6 at 100 3/6 at 150
27	290	<i>20550</i>	23.1	0.11	<b>210</b>	<b>30 / 100 / 300</b>	ET ≥ 30 EW ↑ ≥ 100	LW ↑ ≥ 100 LC ↑ ≥ 100	not done
28	290	<i>14835</i>	<i>420</i>	1.5	> <b>274</b>	<u>7.5 / 25 / 75</u>	ET ≥ 25 EW -	LW ↑ ≥ 25 LC ↑ ≥ 25 <sup>j</sup>	not done
29	339	<i>22980</i>	<i>22.1</i>	0.074	> <b>299</b>	<u>2 / 15 / 100</u>	ET = 100 EW ↑ = 100	LW ↑ = 100 LC ↑ = 100	not done
30	290	<i>8290</i>	63.2	0.21	> <b>300</b>	<i>12.5 / 25 / <u>50</u></i>	-	-	-
31	290 349	<i>89510</i> <i>48480</i>	38.8	0.094	<b>413</b>	<i>10 / <u>30</u> / 100</i>	ET = 100 EW ↑ = 100	LW ↑ = 100 LC ↑ = 100	-
32	352	<i>14860</i>	17.0	0.027	<b>630</b>	<b>50 / 100 / 250<sup>k</sup></b>	ET ≥ 50 EW ↑ ≥ 50	LW ↑ ≥ 50 LC ↑ ≥ 50	1/6 at 100 3/6 at 250
33	335	<i>33900</i>	<i>50.0</i>	0.078	> <b>644</b>	<b>30 / 60<sup>l</sup></b>	ET ≥ 30 EW ↑ ≥ 30	<sup>m</sup>	-
34	290	<i>7990</i>	<i>1000</i>	0.378	> <b>2645</b>	<i>5 / <u>10</u> / 15<sup>n</sup></i>	ET = 15 EW <sup>o</sup>	LW ↑ = 15 LC ↑ = 15 <sup>j</sup>	-

Abbreviations: see Table 1

<sup>a</sup> Numbers in *italics* represent measurements at the lower spectrum cut-off at 290 nm (not at a peak).

<sup>b</sup> The IC<sub>50</sub> values for cytotoxicity in the absence (-irr) and presence (+irr) of irradiation with simulated sunlight are given in this table. Numbers in *italics* represent the highest tested concentration (not IC<sub>50</sub> values), which was limited by solubility or the maximal assay range (1000 µg/mL), thus preventing the determination of exact PIF values (indicated by PIF “larger than”).

<sup>c</sup> Three dose levels (oral gavage, if not indicated differently) were tested and are given in this table; the NOAEL is underlined; the LOAEL is **bolded**.

<sup>d</sup> Ear skin erythema (ET) and weight (EW) changes are described (with dose levels of occurrence in mg/kg).

<sup>e</sup> Lymph node weight (LW) and cell count (LC) changes are described (with dose levels of occurrence in mg/kg).

<sup>f</sup> Incidences at indicated dose levels (in mg/kg) are described

<sup>g</sup> 300 mg/kg/day (drug candidate # 2) / 900 mg/kg/day (drug candidate # 25) toxic (terminated ahead of schedule).

<sup>h</sup> At 50 mg/kg/day (drug candidate # 6) / 100 mg/kg/day (drug candidate # 14) / all dose levels (drug candidate # 21), UV/vis-independent decrease of lymph node parameters.

<sup>i</sup> In a first murine photo-LLNA study, dose levels of 10, 30, and 100 mg/kg/day were tested with no ear, lymph node, or retina finding.

<sup>j</sup> Auricular lymph node hyperplasia also in the absence of irradiation at 75 mg/kg/day (drug candidate # 28) / 15 mg/kg/day (drug candidate # 34), making interpretation difficult.

<sup>k</sup> No irradiation on day 3 due to persisting skin reactions.

<sup>l</sup> Only two dose levels tested.

<sup>m</sup> Reversal of auricular lymph node hypoplasia induced by drug candidate # 33 at  $\geq 30$  mg/kg/day.

<sup>n</sup> intravenous administration (all three dose levels)

<sup>o</sup> Drug candidate # 34 induced increased ear weights in the absence of UV/vis irradiation with no clear effect of UV/vis irradiation on this parameter.

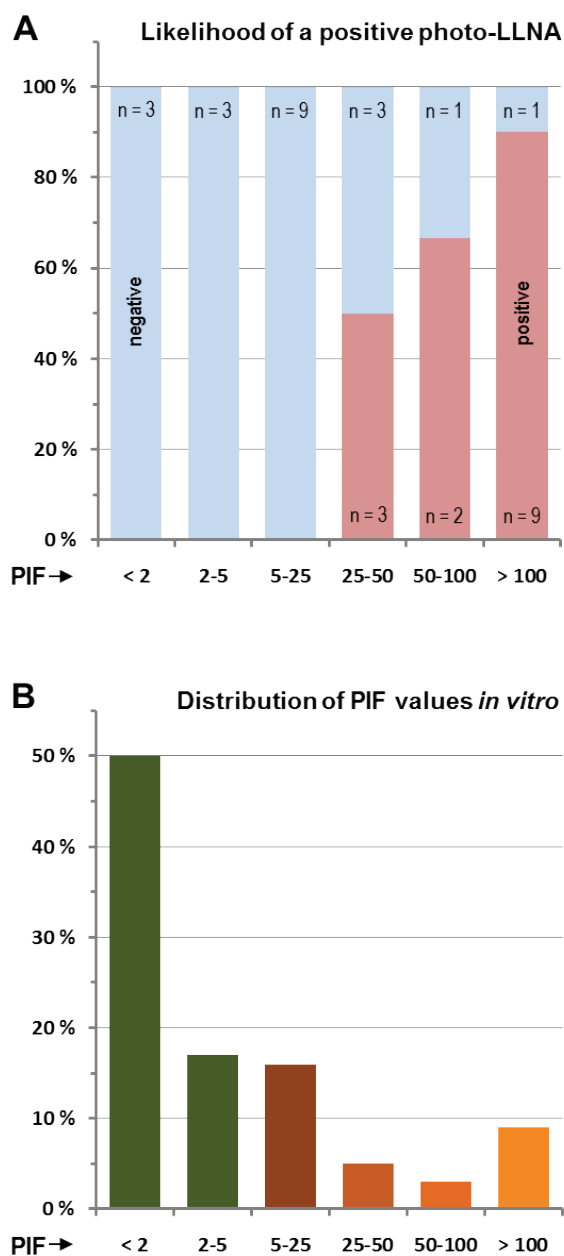


Figure 4: Likelihood of positive test results as a function of the PIF value. **A**, likelihood of a positive outcome in the optimized murine photo-LLNA based on the reported 34 drug candidates; **B**, distribution of PIF values (histogram, n = 100), derived from a historical database of an unbiased selection of drug candidates covering approximately three years of testing

The majority of drug candidates (67 %) had a PIF below 5 and was not considered phototoxic *in vitro*. Moreover, 83 % of all candidates had PIF values below 25, while 8 % of drug candidates showed PIF values between 25 and 100, and further 9 % of drug candidates were highly phototoxic *in vitro* (PIF > 100).

In most cases, signs of ear skin irritation (erythema and/or increased ear biopsy weights) and auricular LN response (increased LN weight and cell count) occurred together. As exceptions, drug candidates # 20, 23, and 27 were characterized by a high sensitivity to irradiation-dependent skin reactions, particularly erythema formation. These started to occur at dose levels, at which local LNs were not responding yet. The most severe case of phototoxicity *in vivo* was associated with drug candidate # 32, characterized by a PIF of 630. In the modified murine photo-LLNA for this orally applied drug candidate, exposure to simulated sun light was not done on day 3 because of persisting compound/irradiation-induced skin reactions.

The use of three dose levels in the modified murine photo-LLNA enabled the establishment of NOAELs and/or LOAELs. As an example, the results of the *in vivo* testing of drug candidate # 26 are shown in **Figure 5** (ear weight and auricular LN responses), **Figure 2** (eye histopathology), and **3B** (erythema formation). No significant ear, LN, or eye response was observed at 50 mg/kg/day, representing the NOAEL with regard to phototoxicity. Irradiation-dependent ear irritation (erythema formation, increased ear biopsy weights),

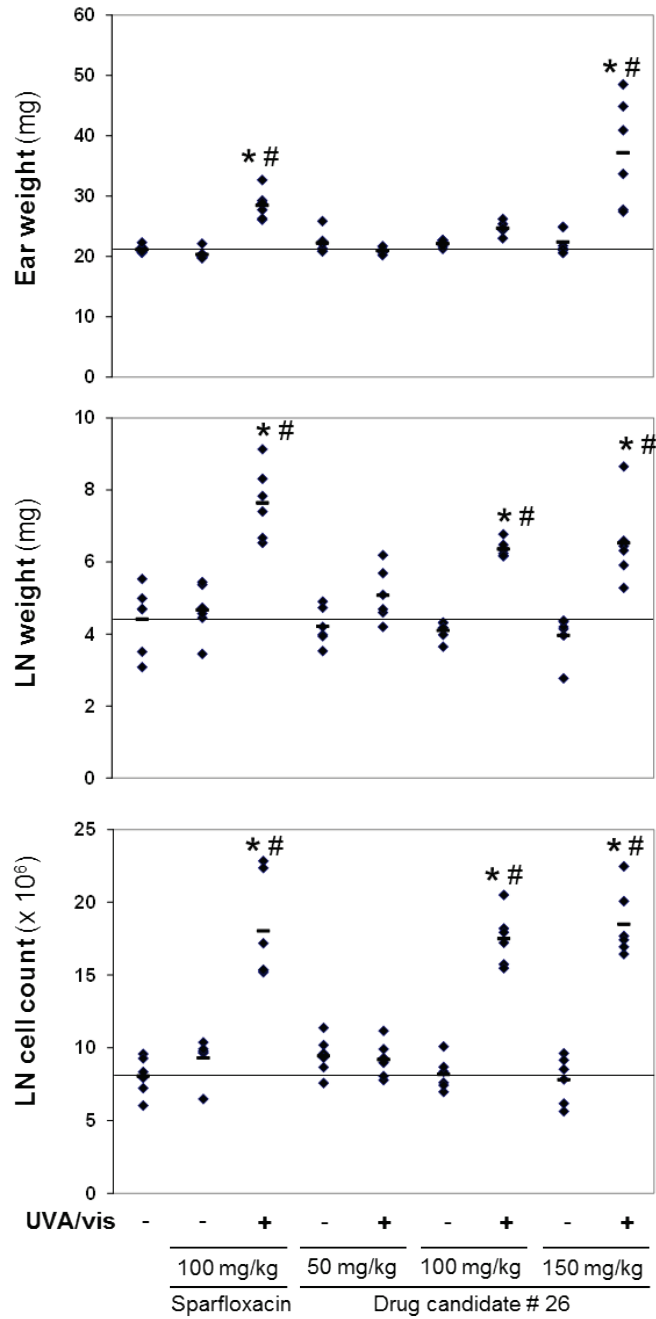


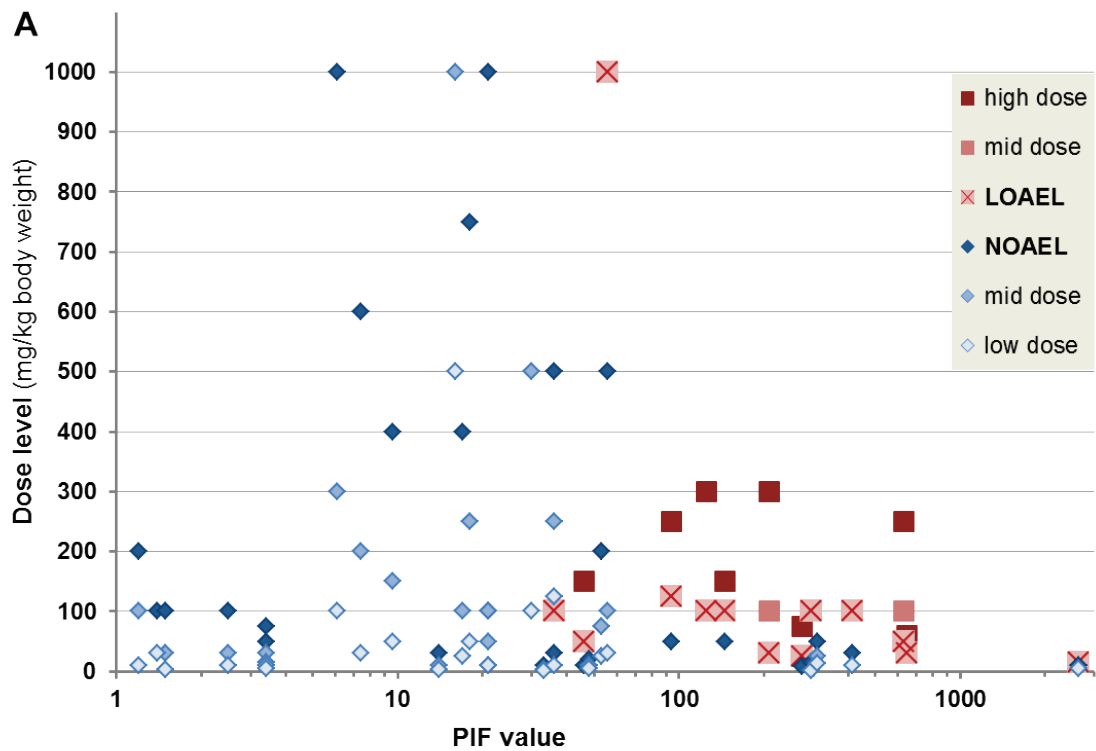
Figure 5: Irradiation-dependent increase of ear weight and auricular LN weight and cell count following oral (gavage) administration of drug candidate # 26 to female BALB/c mice in the modified murine photo-LLNA. \* P < 0.05 vs vehicle control; # P < 0.05 vs corresponding non-irradiated group.

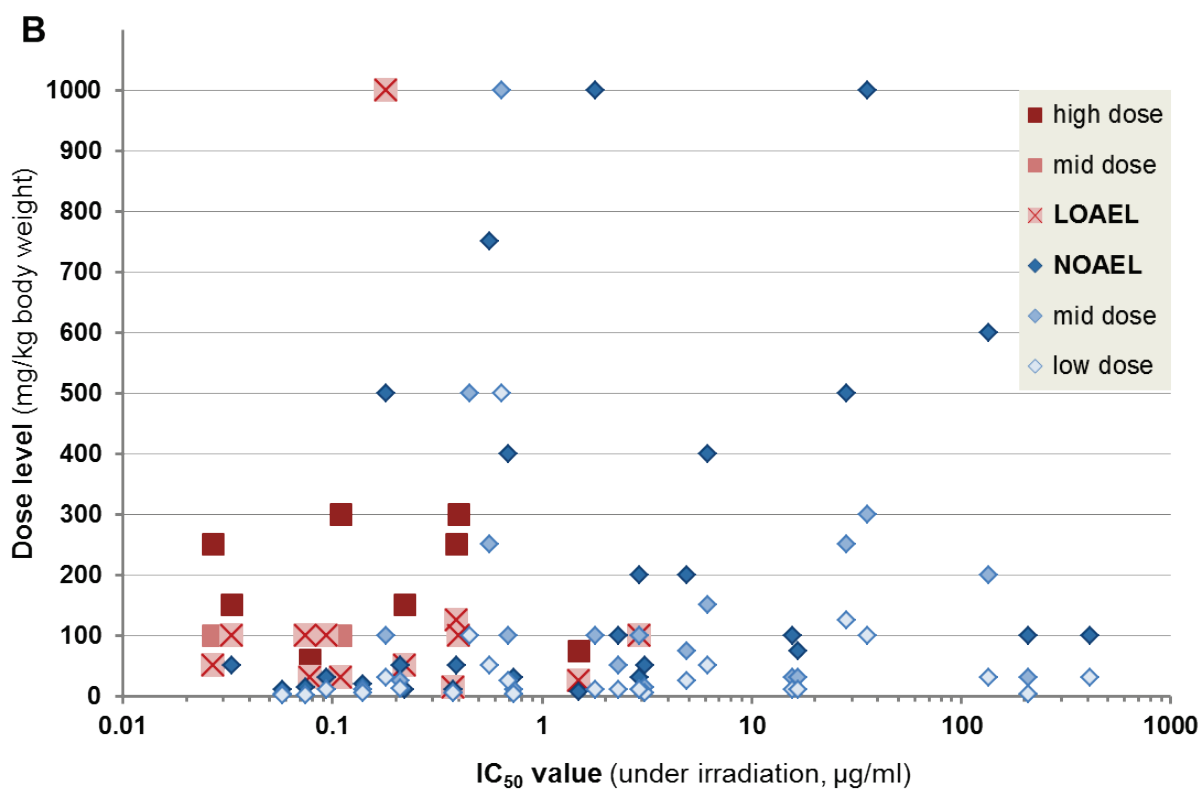
auricular LN response (increased LN weights and cell counts), and minimal to slight atrophy and degeneration of the retina that was qualitatively similar to

changes observed with sparfloxacin and irradiation, became apparent at 100 mg/kg/day (LOAEL) and 150 mg/kg/day. As for sparfloxacin, also in the case of drug candidate # 26 and other drug candidates showing a phototoxic potential *in vivo*, irradiation-dependent erythema formation increased over the treatment period dose-dependently.

**Figure 6A** shows the correlation of the *in vivo* photo-LLNA results with the PIFs of the *in vitro* 3T3 NRU phototoxicity test results. With the exception of compound # 23, the LOAEL for all drug candidates identified as phototoxic in the photo-LLNA was  $\leq 125$  mg/kg/day. Among the 12 drug candidates with a PIF  $\geq 56$ , the only drug candidate that did not show a phototoxic potential was compound # 30, which was tested only up to 50 mg/kg/day. **Figure 6B** shows the correlation of the *in vivo* photo-LLNA results with the IC<sub>50</sub> values of the 3T3 NRU test results. The probability to cause phototoxicity *in vivo* was higher for drug candidates with low IC<sub>50</sub> values. Out of all 24 tested drug candidates with an IC<sub>50</sub> value  $< 3$   $\mu$ M, 13 candidates (= 54 %), and out of all 8 tested drug candidates with an IC<sub>50</sub> value  $< 0.2$   $\mu$ M, 7 candidates (= 88 %) showed a phototoxic potential in the *in vivo* assay.

Figure 6: Correlation of *in vivo* photo-LLNA results with PIF / IC<sub>50</sub> values (*in vitro* 3T3 NRU phototoxicity test). The outcome (positive/negative) of individual dose groups are shown depending on *i.* the dose levels and *ii.* the associated PIF value (A) or IC<sub>50</sub> value (B) (under irradiation) of the tested compound. Thus, all dose groups of a single animal study are vertically stacked above the associated *in vitro* result (A, PIF value; B, IC<sub>50</sub>). The horizontal level indicates the dose level, the symbol indicates the outcome including any identified NOAEL or LOAEL.





## 2.4. Discussion

The clinically relevant phototoxic compounds sparfloxacin, enoxacin, lomefloxacin, doxycycline, 8-MOP and vemurafenib were reliably identified as phototoxic in the herein described optimized modified murine photo-LLNA. These results are in alignment with previous studies including sparfloxacin, enoxacin, lomefloxacin, and 8-MOP in similar *in vivo* murine phototoxicity assays (Matsumoto et al., 2010; Neumann et al., 2005; Vohr et al., 2001). However, whereas enoxacin has been described to exclusively induce irradiation-dependent LN responses but no increase in ear thickness (Vohr et al., 2001), it induced a statistically significant increase of ear biopsy weights in addition to LN responses in our study using the optimized modified murine oral (gavage) photo-LLNA at the same dose level. Furthermore, whereas 8-MOP has been described to induce phototoxicity at 10 mg/kg/day (Neumann et al., 2005; Vohr et al., 2001), 10 mg/kg/day represented the NOAEL and 20 mg/kg/day the LOAEL in our study. Differences in the mouse strain and/or irradiation conditions may explain these differences. Additionally, differences in the chosen endpoints (ear biopsy weight *vs* ear thickness) may have contributed to the described differences regarding irradiation-dependent ear skin reactions to enoxacin. The *in vivo* phototoxic potential of systemically applied ketoprofen could only be identified based on erythema formation at the toxic dose level of 500 mg/kg/day. Clinically, ketoprofen is well known as a phototoxic compound upon topical application (Bagheri et al., 2000). However, only anecdotal cases of ketoprofen-induced phototoxicity upon systemic application have been reported (Foti et al., 2011). Therefore, the modified murine photo-LLNA confirmed the relatively weak potential of ketoprofen to induce phototoxicity upon systemic treatment and

emphasizes the clinically observed difference of ketoprofen-associated phototoxicity risks following topical vs systemic administration. Promethazine, another clinically phototoxic compound upon topical application (Sidi et al., 1955), did not show a phototoxic potential in the modified murine photo-LLNA up to the maximally tolerated dose of 100 mg/kg/day (data not shown). It should be noted that incidence and relevance of phototoxicity seen clinically after oral administration of promethazine remains unclear as well, even though such cases have been reported occasionally (e.g. Epstein and Rowe, 1957; Newill, 1960). Compared to other phenothiazine derivatives the *in vitro* phototoxicity potential of promethazine is slightly below chlorpromazine (photo-hemolysis test, Eberlein-König *et al.*, 1997; *in vitro* 3T3 NRU, in-house data, not shown). However, in mice promethazine showed hardly any phototoxicity reaction after intraperitoneal administration, while chlorpromazine was clearly positive (Ljunggren and Möller, 1977), thus confirming an overall low phototoxicity potential after systemic administration.

Sparfloxacin at a dose of 100 mg/kg/day was chosen as standard positive control item in further murine photo-LLNA studies for drug candidates. This reference compound absorbs visible light in addition to UV light so that it also represents a relevant reference compound with regard to retinal phototoxicity. Indeed, sparfloxacin did not only reliably induce irradiation-dependent local ear irritation and an auricular LN response, but also retina atrophy, a strongly adverse phototoxic effect relevant for systemically applied compounds which absorb light above 400 nm. Histopathological evaluation of the retina for systemically applied compounds absorbing light at > 400 nm represents an important endpoint of the optimized modified murine photo-LLNA.

For lomefloxacin (Matsumoto et al, 2010) as well as for sparfloxacin, doxycycline, ketoprofen, and several drug candidates showing a phototoxic potential in the modified murine photo-LLNA, irradiation-dependent erythema formation increased over the treatment period dose-dependently. This strongly argues for the general need of multiple treatment days rather than only one for *in vivo* systemic phototoxicity testing. The three-day treatment as used here for the modified murine photo-LLNA appears to be appropriate.

*In vivo* phototoxicity is a dose-dependent effect. In addition, photosafety assessment may not only consider the phototoxic potential of a drug candidate but also the relevance for the therapeutic treatment. Therefore, inclusion of multiple dose levels in the *in vivo* phototoxicity test, considering the maximal tolerated and pharmacologically efficacious dose levels with the aim to identify NOAELs and/or LOAELs and potential safety margins *versus* therapeutically relevant drug levels, is important. Since exposure to simulated sun light is done for a limited period of time, determination of drug exposure at the time of irradiation is considered to be relevant for photosafety assessment. Overall, the results obtained with the clinically relevant reference compounds convincingly demonstrate the general suitability of the selected study design including irradiation conditions and endpoints which are in line with current regulatory recommendations (ICH S10, 2013).

An *in vitro* – *in vivo* correlation demonstrated that a drug candidate classified as “phototoxic” *in vitro* based on the 3T3 NRU test is not necessarily phototoxic *in vivo*. However, the probability of a drug candidate to cause phototoxicity *in vivo* clearly correlated with the magnitude of the phototoxicity identified *in vitro*. This

has implications on the preclinical *in vivo* photosafety testing strategy. For example, none of the 15 tested drug candidates, which were characterized by a PIF < 25 showed a phototoxic potential in the modified murine systemic photo-LLNA. Since based on historical data 83 % of all drug candidates fell into this category, *in vivo* efforts early in drug development may primarily focus on the 17 % of drug candidates with a PIF > 25, which were associated with a probability of 68 % to show a phototoxic potential *in vivo*. Most strikingly, this probability increased to 90 % for drug candidates with a PIF > 100. It should be noted that due to inter-laboratory differences regarding the *in vitro* 3T3 NRU phototoxicity test, the mentioned PIF threshold of 25 may not be applicable to other laboratories. Thus, corresponding PIF thresholds need to be identified by laboratories individually.

## 2.5. Conclusion

Taken together, the modified murine photo-LLNA, based on quantification of skin irritation (erythema, ear biopsy weight) and auricular LN weight and cell count, is suitable to support preclinical photosafety assessment of systemically applied drug candidates. For drug candidates absorbing visible light, additional histopathological analysis of the retina is informative and can thus be recommended. The observed increase of erythema formation over the treatment period as well as pharmacokinetic considerations support the need for multiple treatment days, and a three-day treatment design as used in our study seemed appropriate. The establishment of NOAELs and LOAELs is supported by the inclusion of three dose levels. This allows for the calculation of multiples (safety margin) between non-phototoxic and pharmacologically relevant drug levels in order to determine therapeutic indices and support human photosafety assessment.

Since the probability for a drug candidate to cause phototoxicity *in vivo* correlated with the magnitude of the phototoxicity identified *in vitro*, further *in vivo* efforts early in drug development may primarily focus on drug candidates with PIF values above a certain threshold. This PIF threshold needs to be defined individually for each laboratory due to potential inter-laboratory variability, in our case it is 25. For all other drug candidates identified as phototoxic *in vitro*, the *in vivo* photosafety testing may be delayed to a later time point in drug development.

## Acknowledgements

We thank the following Novartis colleagues for their excellent support: W. Dalcher, P. Scheubel, M. Schneider, and M. Spielmann (technical and experimental support); J. Boisclair, E. Perentes, and D.R. Roth (pathology support); D. Brees, M. Kammüller, and U. Plappert-Helbig (scientific support).

## References

- Bagheri, H., Lhiaubet, V., Montastruc, J.L., Chouini-Lalanne, N., 2000. Photosensitivity to ketoprofen: mechanisms and pharmacoepidemiological data. *Drug Saf.* 22, 339-349.
- Bauer, D., Averett, L.A., De Smedt, A., Kleinman, M.H., Muster, W., Pettersen, B.A., Robles, C., 2013. Standardized UV-vis spectra as the foundation for a threshold-based, integrated photosafety evaluation. *Regul. Toxicol. Pharmacol.*, submitted.
- Boudon, S.M., Plappert-Helbig, U., Odermatt, A., Bauer, D., 2013. Characterization of vemurafenib phototoxicity in a mouse model. *Toxicol. Sci.*, doi: 10.1093/toxsci/kft237, first published online: October 23, 2013.
- Bjellerup, M., Ljunggren, B., 1994. Differences in phototoxic potency should be considered when tetracyclines are prescribed during summertime: a study on doxycycline and lymecycline in human volunteers, using an objective method for recording erythema. *Br. J. Dermatol.* 130, 356-360.
- Blank, H., Cullen, S.I., Catalano, P.M., 1968. Photosensitivity studies with demethylchlortetracycline and doxycycline. *Arch. Derm.* 97, 1-2.
- Cohen, J.B., Bergstresser, P.R., 1994. Inadvertent phototoxicity from home tanning equipment. *Arch. Dermatol.* 130, 804-806.

- Correia, O., Delgado, L., 1994. Bullous photodermatitis after lomefloxacin. *Arch. Dermatol.* 130, 808-809.
- Dawe, R.S., Ibbotson, S.H., Sanderson, J.B., Thomson, E.M., Ferguson, J., 2003. A randomized controlled trial (volunteer study) of sitafloxacin, enoxacin, levofloxacin and sparfloxacin phototoxicity. *Br. J. Dermatol.* 149, 1232-1241.
- Dillon, J., Zheng, L., Merriam, J.C., Gaillard, E.R., 2000. Transmission spectra of light to the mammalian retina. *Photochem. Photobiol.* 71, 225-229.
- Drucker, A.M., Rosen, C.F., 2011. Drug-induced photosensitivity. *Drug Saf.* 34, 821-837.
- Eberlein-König, B., Bindl, A., Przybilla, B., 1997. Phototoxic properties of neuroleptic drugs. *Dermatology* 194, 131-135.
- Epstein, S., Rowe, R.J., 1957. Photoallergy and photocross-sensitivity to phenergan. *J. Invest. Dermatol.* 29, 319-326.
- Ferguson, J., 2002. Photosensitivity due to drugs. *Photodermatol. Photoimmunol. Photomed.* 18, 262-269.
- Foti, C., Cassano, N., Vena, G.A., Angelini, G., 2011. Photodermatitis caused by oral ketoprofen: two case reports. *Contact Dermatitis.* 64, 181-183.
- Frank, G. B. and Jhamandas, K. 1970. Effects of drugs acting alone and in combination on the motor activity of intact mice. *Br. J. Pharmac.* 39, 696-706.
- Frost, P., Weinstein, G.D., Gomez, E.C., 1972. Phototoxic potential of minocycline and doxycycline. *Arch. Derm.* 105, 681-683.
- Hamanaka, H., Mizutani, H., Shimizu, M., 1998. Sparfloxacin-induced photosensitivity and the occurrence of a lichenoid tissue reaction after prolonged exposure. *J. Am. Acad. Dermatol.* 38, 945-949.
- Homey, B., von Schilling, C., Blümel, J., Schuppe, H.C., Ruzicka, T., Ahr, H.J., Lehmann, P., Vohr, H.W., 1998. An integrated model for the differentiation of chemical-induced allergic and irritant skin reactions. *Toxicol. Appl. Pharmacol.* 153, 83-94.

- ICH Harmonized Tripartite Guideline S10 “Photosafety evaluation of pharmaceuticals”, 2013.
- <http://www.ich.org/products/guidelines/safety/article/safety-guidelines.html>
- Izu, R., Gardeazabal, J., González, M., Landa, N., Ratón, J.A., Díaz-Pérez, J.L., 1992. Enoxacin-induced photosensitivity: study of two cases. *Photodermatol. Photoimmunol. Photomed.* 9, 86-88.
- Kang, J.S., Kim, T.H., Park, K.B., Chung, B.H., Youn, J.I., 1993. Enoxacin photosensitivity. *Photodermatol. Photoimmunol. Photomed.* 9, 159-161.
- Lapolla, W., Yentzer, B.A., Bagel, J., Halvorson, C.R., Feldman, S.R., 2011. A review of phototherapy protocols for psoriasis treatment. *J. Am. Acad. Dermatol.* 64, 936-949.
- Layton, A.M., Cunliffe, W.J., 1993. Phototoxic eruptions due to doxycycline – a dose-related phenomenon. *Clin. Exp. Dermatol.* 18, 425-427.
- Lei, B., Yao, G., 2006. Spectral attenuation of the mouse, rat, pig and human lenses from wavelengths 360 nm to 1020 nm. *Exp. Eye Res.* 83, 610-614.
- Lipsky, B.A., Dorr, M.B., Magner, D.J., Talbot, G.H., 1999a. Safety profile of sparfloxacin, a new fluoroquinolone antibiotic. *Clin. Ther.* 21, 148-159.
- Lipsky, B.A., Miller, B., Schwartz, R., Henry, D.C., Nolan, T., McCabe, A., Magner, D.J., Talbot, G.H., 1999b. Sparfloxacin versus ciprofloxacin for the treatment of community-acquired, complicated skin and skin-structure infections. *Clin. Ther.* 21, 675-690.
- Ljunggren, B., Möller, H., 1977. Phenothiazine phototoxicity: an experimental study on chlorpromazine and related tricyclic drugs. *Acta Derm. Venereol.* 57, 325-329.
- Man, I., Murphy, J., Ferguson, J., 1999. Fluoroquinolone phototoxicity: a comparison of moxifloxacin and lomefloxacin in normal volunteers. *J. Antimicrob. Chemother.* 43 (Suppl. B), 77-82.
- Matsumoto, N., Akimoto, A., Kawashima, H., Kim, S., 2010. Comparative study of skin phototoxicity with three drugs by an in vivo mouse model. *J. Toxicol. Sci.* 35, 97-100.

- Moore, E.M., 2002. Drug-induced cutaneous photosensitivity. *Drug Saf.* 25, 345-372.
- Neumann, N.J., Blotz, A., Wasinska-Kempka, G., Rosenbruch, M., Lehmann, P., Ahr, H.J., Vohr, H.W., 2005. Evaluation of phototoxic and photoallergic potentials of 13 compounds by different in vitro and in vivo methods. *J. Photochem. Photobiol. B.* 79, 25-34.
- Newill, R.G., 1960. Photosensitivity caused by promethazine. *Br. Med. J.* 30, 359-360.
- NIH publication no. 99-4494, 1999. The murine local lymph node assay: a test method for assessing the allergic contact dermatitis potential of chemicals/compounds.
- OECD guideline for testing of chemicals no. 432, 2004. In vitro 3T3 NRU phototoxicity test.
- Pierfitte, C., Royer, R.J., Moore, N., Bégaud, B., 2000. The link between sunshine and phototoxicity of sparfloxacin. *Br. J. Clin. Pharmacol.* 49, 609-612.
- Sidi, E., Hincky, M., Gervais, A., 1955. Allergic sensitization and photosensitization to phenergan cream. *J. Invest. Dermatol.* 24, 345-352.
- Sliney, D.H., 2002. How light reaches the eye and its components. *Int. J. Toxicol.* 21, 501-509.
- Ulrich, P., Streich, J., Suter, W., 2001. Intralaboratory validation of alternative endpoints in the murine local lymph node assay for the identification of contact allergic potential: primary ear skin irritation and ear-draining lymph node hyperplasia induced by topical chemicals. *Arch. Toxicol.* 74, 733-744.
- Ulrich, P., Vohr, H.W., 2012. Utilization of irritation data in the local lymph node assay, in: Wilhelm, K.P., Zhai, H., Maibach, H.I. (Eds.), *Dermatotoxicology*. Informa Healthcare, London, pp. 306-312.
- Van den Broeck, W., Derore, A., Simoens, P., 2006. Anatomy and nomenclature of murine lymph nodes: descriptive study and nomenclatory standardization in BALB/cAnNCrI mice. *J. Immunol. Methods* 312:12-19.

Vohr, H.W., Blümel, J., Blotz, A., Homey, B., Ahr, H.J., 2001. An intra-laboratory validation of the integrated model for the differentiation of skin reactions (IMDS): discrimination between (photo)allergic and (photo)irritant skin reactions in mice. Arch. Toxicol. 73, 501-509.

### 3. Characterization of Vemurafenib Phototoxicity in a Mouse Model

**Boudon, S.M., Plappert-Helbig, U., Odermatt, A., Bauer, D. 2013. Characterization of Vemurafenib Phototoxicity in a Mouse Model. *Tox. Sci.* doi: 10.1093/toxsci/kft237**

**First published online: October 23, 2013**

**This work was presented at the 14<sup>th</sup> Annual XeRR Meeting 2013. Zürich, Switzerland, Dec. 2013.**

#### Abbreviations

8-MOP	8-methoxypsoralen
CMC	carboxymethylcellulose
DMEM	Dulbecco's modified eagle medium
HBSS	Hank's Buffered Salt Solution
LC-MS	liquid chromatography - mass spectrometry
LLNA	local lymph node assay
LOAEL	lowest observed adverse effect level
MED	minimal erythematous dose
NOAEL	no observed adverse effect level
NRU	neutral red uptake
UPLC	ultrahigh-performance liquid chromatography
UV	ultraviolet

## Abstract

Vemurafenib is a first-in-class, small molecule B-Raf kinase inhibitor for the treatment of patients with unresectable or metastatic melanoma carrying the BRAFV600E mutation, commercially available since 2011. A general phototoxic potential was identified early during development; however based on results of an animal study in hairless rats, it was concluded that there would exist no relevant risk for humans. Surprisingly, signs of clinical photosensitivity were reported in many patients during clinical development. Therefore, it became a fundamental question to understand this discrepancy.

An established mouse model (oral UV-Local Lymph Node Assay, UV-LLNA) for the assessment of in vivo photosafety was used to investigate the impact of formulations, dose levels, duration of treatment and timing of irradiation. Moreover a basic pharmacokinetic profile was established within the same mouse strain.

We were able to demonstrate dose- and time-dependent phototoxicity of vemurafenib using commercially available tablets (stabilized amorphous material). The lowest phototoxic dose was 350 mg/kg administered for three consecutive days followed by exposure to UV-visible irradiation at a UVA-normalized dose of 10 J/cm<sup>2</sup>. In comparison, pure vemurafenib, which easily forms crystalline variants and is known to have poor bioavailability, was tested at 350 mg/kg and no signs of phototoxicity could be seen. The most apparent difference between the early study in hairless rats and the current study in mice was the spectral range of the irradiation light source (350 to 400 nm versus 320 to 700 nm). Since vemurafenib does not absorb sufficiently light above 350 nm, this difference can easily explain the negative earlier study result in hairless rats.

Keywords:

Phototoxicity, Photosensitivity, Photosafety, LLNA, BRAF, Vemurafenib

### 3.1. Introduction

Vemurafenib is a first-in-class, small molecule B-Raf kinase inhibitor for the treatment of patients with unresectable or metastatic melanoma carrying the BRAFV600E mutation. It was approved in 2011 in the United States (FDA review, 2011), in the European Union (CHMP review) and in Switzerland.

Although a general phototoxic potential was identified early for this compound (based on UV-vis spectra and in vitro 3T3 Neutral Red Uptake (NRU) phototoxicity data) the initial conclusion was made that no relevant human risk would exist. Apparently, this was driven by the results of an animal study suggesting that no increased sensitivity to light could be induced (FDA review 2011, CHMP review 2011). Surprisingly, signs of clinical photosensitivity were reported in 42 % of patients included in the Phase I trial extension cohort. Similarly, during Phase II and Phase III, 52 % and 30 % of vemurafenib-treated patients were affected, respectively (Chapman *et al.*, 2011; Flaherty *et al.*, 2010, Lacouture *et al.* 2013). The findings included severe (grade 2 and 3) sun-burn-like reactions, which occurred even after exposure to sun light through window glass (*e.g.* while driving a car) and, thus, had a significant impact on the quality of life. Later, Dummer *et al.* (2012) confirmed that the minimal erythema dose (MED) in patients receiving vemurafenib was markedly reduced in the UVA range, while the UVB-dependent MED remained unchanged when compared to untreated subjects. Therefore, we felt encouraged to understand the reasons behind this situation that a clinically relevant strong phototoxicity had gone undetected preclinically. In particular, it was of great interest to learn how such potentially “false negative” animal studies can be avoided in the future.

In the present study we utilized an established mouse model for the assessment of *in vivo* photosafety. This model is based on a modified (cell count-based) UV-Local Lymph Node

Assay (UV-LLNA) in albino Balb/c mice as described by Ulrich *et al.* (2001). However, with oral administration, the main endpoint of this model is acute phototoxicity rather than (photo)-contact allergy. A similar approach was also described by Vohr *et al.* (2000). Typically, mice were treated for three days including daily exposure to simulated sun light. The light source used provided a reasonable coverage of the UVA and visible light range, while highly cytotoxic UVB irradiation was attenuated in order to not limit the overall irradiation (which was normalized to a UVA dose of 10 J/cm<sup>2</sup> UVA). Any skin reactions (mainly erythema seen at the ears) were recorded during these days. Subsequently, edema (by measuring ear weight) and markers of local inflammation (weight and cell count of the ear-draining auricular lymph nodes) were assessed. Historically, a treatment period of three days has been used to allow for sufficient activation of the local lymph nodes. However, in the context of photosafety evaluation of systemically administered drugs the repeated-dose protocol does also ensures sufficient distribution of compounds to skin.

During clinical development of vemurafenib it became apparent that reaching sufficient systemic exposure in patients was a key challenge, because this drug substance is practically insoluble in an aqueous environment. Finally, solubility was improved by using a stabilized amorphous variant of vemurafenib. This solid dispersion contains amorphous vemurafenib and hypromellose acetate succinate (HPMCAS) in which the drug substance is uniformly dispersed within the polymeric substrate. Currently, the approved daily dose of vemurafenib is 1920 mg (which equals twice daily 4 tablets containing 240 mg each) (Bollag G *et al.*, 2010; Shah *et al.*, 2013). Since reaching sufficient bioavailability is also a key challenge in animal studies with vemurafenib, we performed our experiments with both crystalline and stabilized amorphous material in order to test different conditions. In addition, a pharmacokinetic profile was established within the same mouse strain in order to support

comparisons with published exposure data from both non-clinical safety studies in animals and human clinical trials.

## 3.2. Material and methods

### 3.2.1. Test compounds and positive and negative control items

For most animal studies amorphous vemurafenib was used, which was commercially available as ZELBORAF® tablets (240 mg/tablet, Roche, Basel, Switzerland). Prior to immediate dosing the tablets were fine grinded with a pestle and a mortar. An appropriate amount of aqueous carboxymethylcellulose (CMC) 0.5 % was added to form a fine suspension (final dosage volume of 20 mL/kg) which was sonicated without heating for 5 minutes and shaken/vortexed. The vehicle, CMC 0.5 %, was used as control.

In addition, in-house synthesized vemurafenib was used, mainly for experiments requiring solutions (*e.g.* recording of UV-vis spectra, *in vitro* 3T3 phototoxicity test). This material was assumed to be composed of crystalline forms, which are obtained from chemical synthesis if no special precautions are taken. Identity was confirmed based on <sup>1</sup>H-NMR, LC-MS and UPLC. The obtained data is in agreement with the known structure of vemurafenib. Purity was assessed using UPLC demonstrating 98 % content with ethyl acetate as major remaining impurity.

Sparfloxacin, and 8-methoxypsoralene (8-MOP), used as positive control reference compounds, were obtained from Sigma Aldrich (Buchs, Switzerland) with at least 98 % purity and available certificates of analysis.

### 3.2.2. UV-visible light absorption spectra

Light absorption spectra in the UV-visible range were recorded on a Cary 300 spectrophotometer (Varian Australia Pty Ltd, Mulgrave, Australia) using UV-transparent quartz glass cuvettes (1 cm path length). Substances were dissolved in methanol applying individual solvent-specific baseline correction.

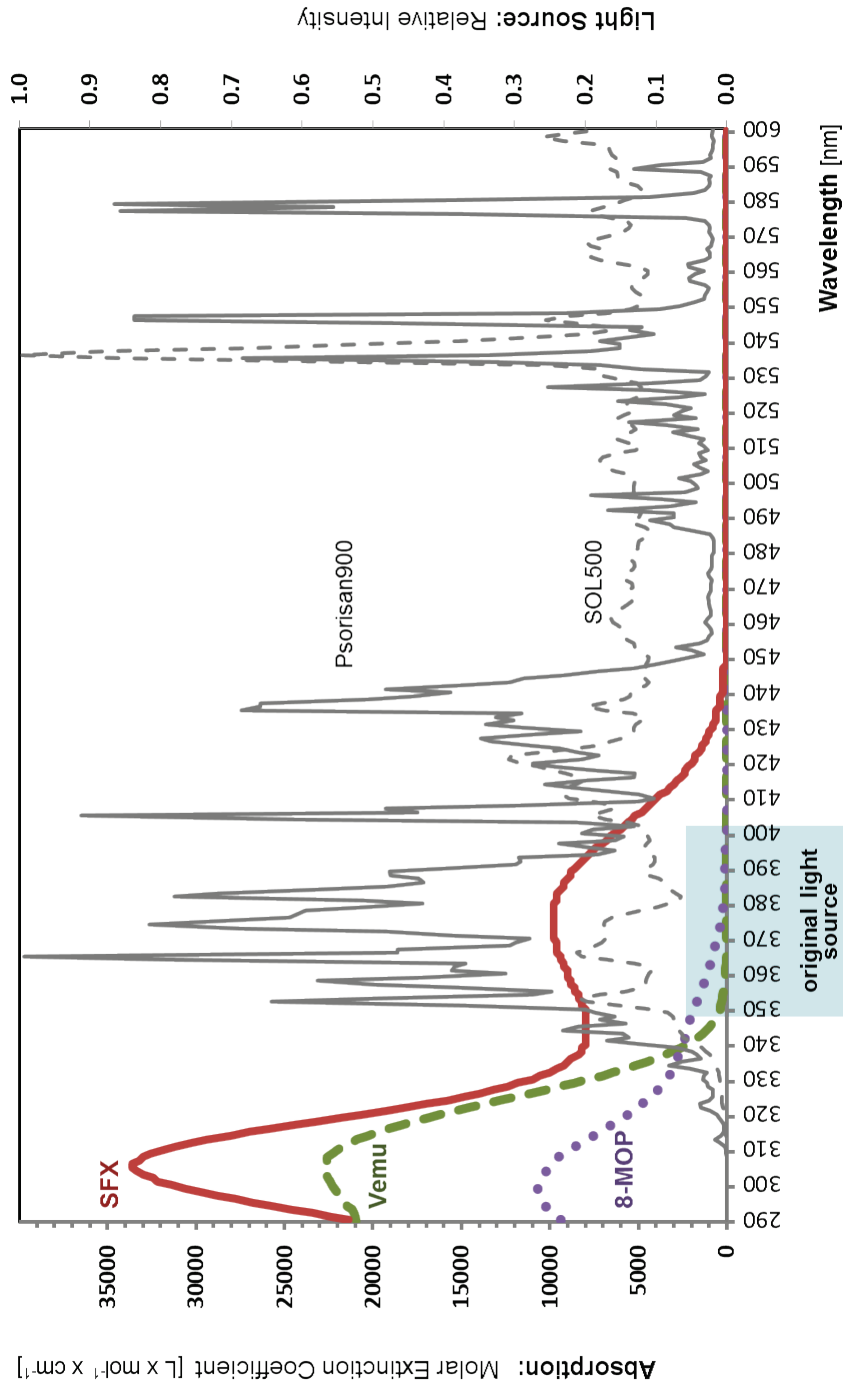
For each peak the molar extinction coefficient ( $\epsilon$  or MEC) was calculated:  $\epsilon = A / (c \times l)$

A: absorbance, c: concentration of the solution in methanol, l: path length (cuvette)

### 3.2.3. In vitro 3T3 neutral red uptake phototoxicity test

The Balb/c mouse fibroblast cell line 3T3.A31 was obtained from the European Collection of Cell Cultures (ECACC, no. 86110401, at passage 82), United Kingdom. Cells were cultivated in Dulbecco's Modified Eagle Medium (DMEM) (with phenol red) containing 10 % fetal calf serum, 1 % glutamine and 1 % penicillin/streptomycin. The assay was performed in accordance with OECD Testing Guideline 432 (2004). Briefly, twenty-four hours after seeding the mouse fibroblast cells into 96-well plates, the medium was removed and the cells were treated with different concentrations of the test compound for 1 h using Hank's Buffered Salt Solution (HBSS) without phenol red as medium replacement. Subsequently these cells were irradiated (+Irr) with simulated sun light (SOL 500 H1, Dr.Hönle GmbH, Gräfelfing, Germany) with a main spectral output from 320 until beyond 700 nm. The integrated H1 filter system attenuated the highly cytotoxic UVB range to a level which was tolerated by the cell culture as suggested by the mentioned guideline. (**Figure 1**) The polystyrene lids were on the 96-well plates during light exposure. Calibration was performed through the lids as well. In parallel, an identically prepared 96-well plate was kept in the dark (-Irr), serving as control.

Fig 1. Normalized UV-visible light absorption spectra of vemurafenib (Vemu, dashed), sparfloxacin (SFX, solid) and 8-methoxypsoralene (8-MOP, dotted) recorded at concentrations of 50  $\mu\text{M}$  or 100  $\mu\text{M}$  in methanol. For comparison the spectral intensity of the light sources used in this study are shown as overlap (SOL500, dashed gray, Psorisan900 solid grey).



UVA irradiance was measured by a UVA meter (Dr. Hönle AG, Gräfelfing, Germany) with spectral sensitivity in the range from 320 to 400 nm and a measuring range between 0 and 199.9 mW/cm<sup>2</sup>. The applied intensity was 1.67 mW/cm<sup>2</sup> resulting in a total UVA dose of 5 J/cm<sup>2</sup> after 50 minutes of irradiation. The related UVB exposure (calculated from the spectral irradiance of the light source) was around 15 mJ/cm<sup>2</sup>. After irradiation the HBSS buffer was replaced by fresh medium. Cell viability was determined 24 h later using neutral red as the vital dye, which was measured after incubation at 540 nm and extraction. The Photo-Irritation-Factor (PIF) was calculated according to OECD TG 432 using the following equation:  $PIF = IC_{50}(-Irr) / IC_{50}(+Irr)$ .

### 3.2.4. Animal experiments

#### 3.2.4.1. Animal husbandry

Female BALB/C mice aged of about 8 weeks at the start of the experiment, purchased from Charles River (L'Arbresle, France), were acclimatized for around one week. The experiments were performed in conformity with the Swiss Animal Welfare Law and in accordance with internal SOPs and guidelines for care and use of laboratory animals. Animals had *ad libitum* access to pelleted standard rodent diet and tap water from the domestic supply and were kept in an air-conditioned animal room under periodic bacteriological control, at 22°C ± 2°C with monitored 30 % - 80 % humidity, a 12 hour light/dark cycle and background radio coordinated with light hours.

#### 3.2.4.2. Irradiation conditions for animal experiments

During irradiation mice were kept in specific cages allowing only for lateral movements and ensuring a uniform irradiation of their back and ears. Non-irradiated animals were kept in their housing cages under standard room light. For irradiation a sun light simulator (Psorisan 900 H1, Dr.Hönle GmbH, Gräfelfing, Germany) was used showing a main spectral output from 320 until beyond 590 nm. The integrated H1 filter system attenuated the highly cytotoxic UVB range to a level which was tolerated by the animals. UVA irradiance was measured by a UV-radiometer (Dr.Hönle GmbH, Gräfelfing, Germany) with a spectral sensitivity in a range from 320 to 400 nm and a measuring range between 0 and 199.9 mW/cm<sup>2</sup>. Typically, the applied intensity was 4.8 mW/cm<sup>2</sup> at a distance of 50 cm. Irradiation was normalized to a dose of 10 J/cm<sup>2</sup> UVA which was typically achieved after 35 minutes of light exposure. The related UVB exposure (calculated from the spectral irradiance of the light source) was around 30 mJ/cm<sup>2</sup>. External calibration of the equipment was performed by Opto.cal GmbH (Movelier, Switzerland) which is a calibration laboratory accredited by the Swiss Accreditation Service.

#### 3.2.4.3. Treatment protocols and endpoints

##### 3.2.4.3.1. Oral UV-Local Lymph Node Assay in BALB/c mice

**Studies A, B and C:** On three consecutive days, six mice per group were treated orally with the test compound (see **Table 1** and **Figure 2** for details) dissolved in 0.5 % aqueous carboxymethylcellulose (CMC) or with vehicle. Two hours after each treatment, mice from the groups “with UV” were irradiated.

Table 1. Skin irritation and LN activation induced by vemurafenib (Vemu) using crystalline and amorphous material (amorph.). Six female Balb/c mice per group were treated orally on three consecutive days by gavage. Mean ear weights were obtained 1 day after the last exposure using the weights of circular pieces (0.5 cm<sup>2</sup>) punched from the apical area of one ear. Mean lymph node (LN) weights were derived from pairs of auricular LN from an individual animal and mean LN cell count values represent the corresponding total cellularity of the LN. \* 1% < P < 5%, \*\*0.1% < P < 1%, \*\*\*P < 0.1%, vs corresponding dose control. Data of the positive control, sparfloxacin, are displayed to illustrate the expected responses for each endpoint.

Study		Ear weights		LN weights		LN cell count		Erythema after UV exposure (day 1/2/3)
		Mean (mg)	SD	Mean (mg)	SD	Mean (x 10 <sup>6</sup> )	SD	
<b>A</b>	Sparfloxacin 100 mg/kg	19.26	0.58	4.44	0.52	8.11	1.66	-
	Sparfloxacin 100 mg/kg <b>UV</b>	***30.72	1.63	***9.45	1.11	***20.60	2.37	+ / + / +
<b>B</b>	Vehicle CMC 0.5%	24.55	1.54	5.99	0.97	9.96	2.24	-
	Vemu crystal 20 mg/kg	20.03	0.62	5.99	0.99	11.78	1.66	-
	Vemu crystal 20 mg/kg <b>UV</b>	20.87	0.86	5.18	0.91	9.77	2.86	- / - / -
	Vemu crystal 100 mg/kg	20.62	0.57	5.48	0.79	10.19	1.50	-
	Vemu crystal 100 mg/kg <b>UV</b>	20.69	0.68	6.51	0.79	11.99	1.01	- / - / -
	Vemu crystal 350 mg/kg	20.98	0.38	5.90	1.12	11.86	2.75	-
	Vemu crystal 350 mg/kg <b>UV</b>	21.25	0.6	6.11	0.69	11.95	1.84	- / - / -
<b>C</b>	Vehicle CMC 0.5%	20.33	0.6	4.23	0.41	5.85	0.42	-
	Vemu amorph 100 mg/kg	21.41	0.89	4.61	0.41	6.18	0.65	-
	Vemu amorph 100 mg/kg <b>UV</b>	21.73	0.49	4.85	0.27	7.48	1.13	- / - / -
	Vemu amorph 450 mg/kg	20.66	0.46	4.58	0.33	7.68	0.87	-
	Vemu amorph 450 mg/kg <b>UV</b>	22.02	0.36	4.63	0.77	7.56	1.40	- / - / +
	Vemu amorph 800 mg/kg	20.65	1.04	4.50	0.77	7.53	1.98	-
	Vemu amorph 800 mg/kg <b>UV</b>	22.13	0.95	4.97	1.14	9.28	1.23	- / - / +
<b>D</b>	Vemu amorph 350 mg/kg	21.12	0.40	5.07	0.33	5.72	0.59	-
	Vemu amorph 350 mg/kg <b>UV</b>	21.11	0.46	5.69	0.94	6.58	1.08	- / - / +
	Vemu amorph 450 mg/kg <b>UV</b> (UV on day 3 only)	20.70	0.39	5.35	1.12	6.81	1.50	- / - / +
<b>E</b>	Vehicle CMC 0.5%	21.57	0.84	-	-	-	-	-
	(6h) Vemu amorph 350 mg/kg	21.43	0.94	-	-	-	-	-
	(1h) Vemu amorph 350 mg/kg <b>UV</b>	**23.55	0.71	-	-	-	-	- / - / +
	(2h) Vemu amorph 350 mg/kg <b>UV</b>	**23.48	0.77	-	-	-	-	- / - / +
	(3h) Vemu amorph 350 mg/kg <b>UV</b>	***24.00	0.84	-	-	-	-	- / - / +
	(4h) Vemu amorph 350 mg/kg <b>UV</b>	**23.82	0.83	-	-	-	-	- / - / +
	(6h) Vemu amorph 350 mg/kg <b>UV</b>	***24.31	1.25	-	-	-	-	- / - / +

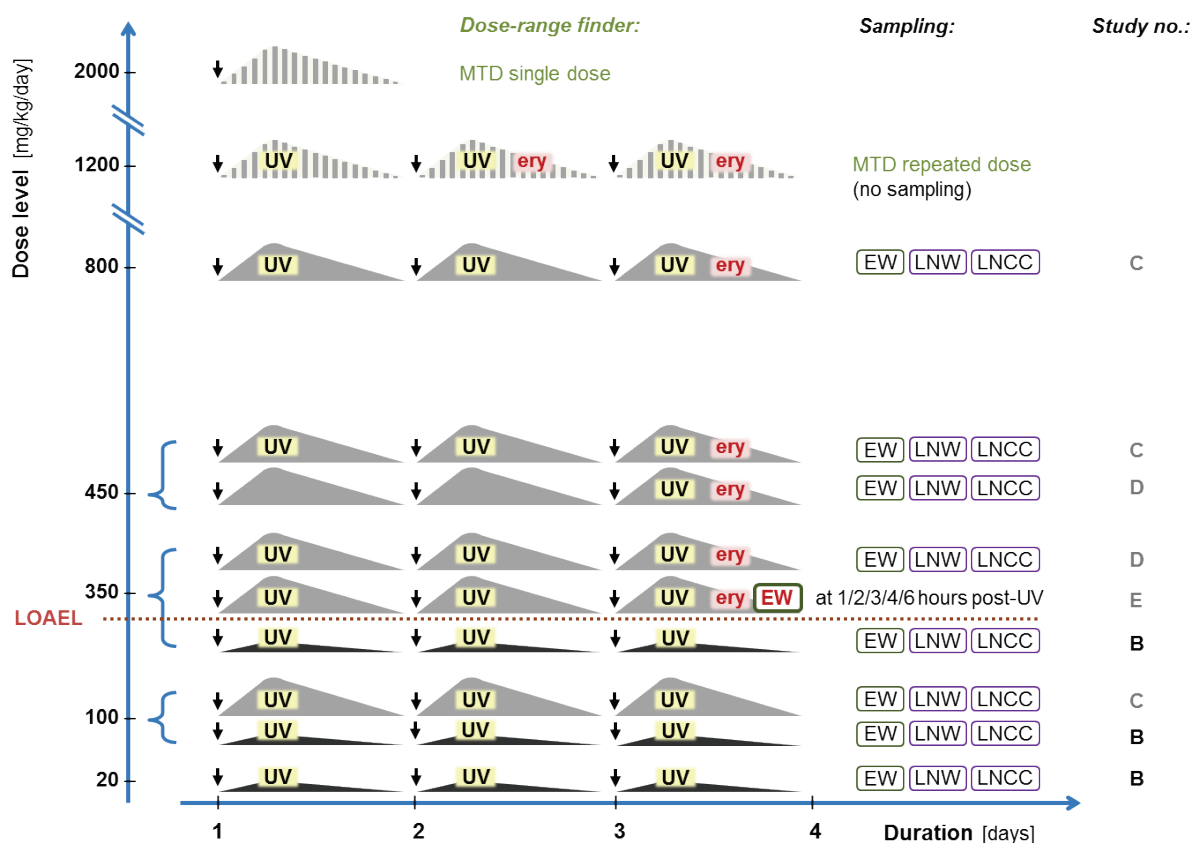


Fig 2. Schematic overview of *in vivo* phototoxicity studies performed with two different variants of vemurafenib (crystalline (black) and amorphous (grey)). The maximum tolerated dose (“MTD”) was assessed in dose finding experiments using individual animals (dashed grey). The shape of the grey and black figures intends to reflect the temporal profile of vemurafenib’s concentration in blood. For the main studies (solid grey or black), two groups of six female BALB/c mice were allocated to each dose, one with and one without subsequent exposure to simulated sun light (“UV”). During the treatment phase, typically daily administration (arrow) during 3 consecutive days, erythema (“ery”, if observed) was monitored during the first six hours following daily irradiation. At necropsy mean ear weights (**EW**, bold red if significantly increased) were calculated using the weights of circular pieces (0.5 cm<sup>2</sup>) punched from the apical area of each ear. Mean lymph node weights (**LNW**) were derived from pairs of auricular lymph nodes and mean lymph node cell count (**LNCC**) values represent the corresponding total cellularity of the lymph node. The red dashed line defines the lowest-observed-adverse-effect-level (LOAEL).

**Study D:** On three consecutive days, six mice per group were treated orally with 350 mg/kg or 450 mg/kg of the amorphous form of vemurafenib. Mice from the 350 mg/kg “with UV” group were irradiated two hours after each treatment while mice from group 450 mg/kg “with UV” were irradiated two hours after last treatment only on day 3.

Measurement of LLNA endpoints was done as described before (Ulrich et al. 2001): 24 h after the last irradiation, mice were sacrificed using carbon dioxide asphyxiation. Circular biopsies (0.5 cm<sup>2</sup>) from the apical area of each ear were excised using a disposable punch and weighed as pairs on an analytical scale. Lymph node weights were obtained from lymph node pairs taken from individual animals and weighed using analytical scales. For the determination of individual lymph node cell counts, single-cell suspensions from the lymph node pairs from individual animals were prepared by mechanical tissue disaggregation through a sterile stainless steel gauze in 1 ml phosphate-buffered saline PBS (Ca<sup>2+</sup>/Mg<sup>2+</sup> -free) containing 0.5% bovine serum albumin BSA. Individual cell counts were determined in a cell counter (CASY<sup>®</sup>TTC cell counter, Schärfe System, Reutlingen, Germany) gating on a particle diameter above 4.88 µm.

#### 3.2.4.3.2. Time-profile of erythema and edema formation after irradiation

**Study E:** On three consecutive days, six mice per group were treated orally with 350 mg/kg of the amorphous form of vemurafenib or with vehicle. Mice were irradiated two hours after each treatment and sacrificed at 1 h, 2 h, 3 h, 4 h and 6 h after light exposure on day 3. Circular biopsies (0.5 cm<sup>2</sup>) from the apical area of each ear were excised using a disposable punch and weighed as pairs on analytical scales.

#### 3.2.4.3.3. Pharmacokinetic profile of vemurafenib in BALB/c mice

On three consecutive days, six mice per group were treated orally with a suspension of the amorphous form of vemurafenib. Blood samples from three animals per time point per group were collected from the vena saphena 1 h, 2 h, 4 h and 7 h post-dosing; blood specimens from six mice per time point per group were collected from terminal heart puncture at 24 h after treatment on day 1 for animals from group 1, on day 2 for animals from group 2, and on day 3 for animals from group 3. Plasma was prepared from blood specimens and stored on ice water until all plasma specimens were prepared. Specimens from all animals were analyzed. 24 h after the administration on day 1, 2 and 3, mice were sacrificed using carbon dioxide asphyxiation. Circular biopsies ( $= 0.5 \text{ cm}^2$ ) from the apical area of each ear were excised using a disposable punch and weighed as pairs on an analytical scale. They were snap-frozen in liquid nitrogen and stored in a deep freezer at  $-70 \text{ }^\circ\text{C}$  or below. Determination of vemurafenib in mouse plasma was performed by protein precipitation followed by LC-MS/MS using electrospray ionization in positive mode. The ear samples were homogenized with nine volume equivalents of acetonitrile/water, then processed and analyzed like the plasma samples.

#### 3.2.4.4. Statistical analysis

For all statistical calculations SigmaPlot for Windows (version 11.0) was used. A One-Way-Analysis-of-Variance was used as the statistical method (Glantz SA, 1992). A normality test was performed to assure that the specimens were drawn from a normal population (significance level = 0.01). The equal variance test was used to check the assumption that the sample was drawn from populations with the same variance (significance level = 0.01). In case of significant results of the One-Way-ANOVA, multiple comparisons were performed

with the Student-Newman-Keuls test. If the normality test and/or the equal variance test gave P values < 0.01, a suitable transformation (log, square root) was applied; if the normality test and/or equal variance test still gave P values < 0.01, the non-parametric Kruskal-Wallis test was used and multiple comparisons for the ranks of the original observations were performed. The confidence interval for the difference of the means was set to 95 % ( $\alpha= 0.05$ ).

### 3.3. Results

#### 3.3.1. UV-visible light absorption spectra

UV-visible spectra of vemurafenib and the reference compounds sparfloxacin and 8-methoxy psoralene were recorded from 290 to 700 nm, which is the spectral region relevant for photosafety assessment (sun light) (**Table 2**). Vemurafenib shows absorption mainly in the UVB (peak at 305 nm) and the short UVA region. Importantly, above 350 nm no relevant absorption is observed. In comparison, 8-MOP shows a similar absorption profile (peak at 299 nm), but absorption extends into the long UVA region up to 380 nm. Sparfloxacin, shows an additional peak (375 nm) in the long UVA and absorption extends into the visible region up to 440 nm. For comparison, an overlay of these absorption spectra with the spectral irradiance of the light sources (*in vitro*: SOL500 / H1 filter, *in vivo*: Psorisan900 / H1 filter) is shown up to 600 nm in **Figure 1**. It should be noted that the obvious absorption of all three compounds in the UVB range is a common phenomenon among the majority of low molecular weight drug substances. However, for oral drugs photosafety assessment is mainly focusing on UVA and visible light as these wavelengths are penetrating sufficiently into skin (ICH S10, step 2 draft, 2012).

Compound	MEC [ L x mol <sup>-1</sup> x cm <sup>-1</sup> ]	Precipitation [ µg / mL ]	IC <sub>50</sub> (-Irr) [ µg / mL ]	IC <sub>50</sub> (+Irr) [ µg / mL ]	PIF
Vemurafenib	22800 (305 nm)	> 1.50	---	0.052	> 29
Sparfloxacin	33600 (305 nm)	> 500	---	6.16	> 82
8-methoxy psoralene	10700 (299 nm)	> 100	---	0.22	> 457

Table 2. Summary of spectrophotometric and *in vitro* phototoxicity data for vemurafenib, and for the reference compounds sparfloxacin and 8-methoxypsoralene.

### 3.3.2. In vitro phototoxicity test results

The *in vitro* 3T3 NRU phototoxicity test measures cytotoxicity profiles in the presence or absence of simulated sun light using neutral red as vital dye. This assay is based on the calculation of the Photo-Irritation Factor (PIF) which represents the ratio of the IC<sub>50</sub> values obtained with (+Irr) or without (-Irr) irradiation. According to the respective OECD Testing Guideline 432 compounds showing a PIF value above 5 (which equals a 5-fold shift of the IC<sub>50</sub> value towards lower concentrations) are considered to be phototoxic. Vemurafenib (**Table 2**) was insoluble in cell culture buffer at concentrations higher than 1.5 µg/mL without showing significant cytotoxicity up to this concentration. However, in the presence of simulated sun light a defined cytotoxicity profile was obtained (IC<sub>50</sub> value of 0.052 µg/mL). The resulting PIF value was 29 (using the solubility limit of 1.5 µg/ml since no IC<sub>50</sub> was obtained in the absence of irradiation), indicating that vemurafenib was clearly phototoxic *in vitro* to cultured cells. In addition, *in vitro* phototoxicity results for sparfloxacin and 8-MOP are shown. PIF values for both compounds are limited by solubility as well. However,

achieved concentrations were significantly higher which resulted in much higher PIF values. Under these conditions, the extremely low  $IC_{50}$  value of vemurafenib (0.052  $\mu\text{g/mL}$ ) illustrates the potent inherent photoreactivity while the solubility-limited PIF value of 29 is likely an underestimate of the true phototoxic potential.

### 3.3.3. Oral UV-Local Lymph Node Assay

Data obtained with the positive control sparfloxacin are displayed in **Table 1** (study A) to illustrate the expected responses for each endpoint. After oral administration of sparfloxacin (100 mg/kg) redness of the ears (erythema) was observed after each irradiation. At the time of necropsy increased ear weight (edema) and a proliferation response in the ear-draining auricular lymph nodes was seen.

For vemurafenib (**Figure 2**), the maximum tolerated dose (MTD) was established at 800 mg/kg in a dose-finding experiment using individual animals. Clinical symptoms were monitored during the dose-finding experiment which started at a dose of 2000 mg/kg body weight/day using amorphous material (finely grinded tablets). Following the first administration reduced activity, piloerection and hunched posture were observed during the initial 5 hours. In concordance with Mackay *et al* (1992), 1200 mg/kg was used as the next lower dose. Similar symptoms, although less pronounced, were observed allowing for additional irradiation after treatment. During the second and third day of treatment, erythema at the ear skin was observed. The next lower dose, 800 mg/kg, was well tolerated by mice for three days (apart from the irradiation-dependent erythema on day 3) and, therefore was regarded as the MTD for amorphous vemurafenib to be considered in subsequent studies.

The oral UV-LLNA with vemurafenib was performed with doses of 20, 100 and 350 mg/kg of crystalline material and with doses of 100, 350, 450 and 800 mg/kg of amorphous material (**Table 1**, respectively studies B, C and D). After oral administration of crystalline vemurafenib no clinical signs and no redness of the ears was observed and the ear-draining lymph nodes showed no proliferation response. After oral administration of amorphous vemurafenib, signs of phototoxicity (erythema) appeared on day 3 directly after UV-exposure at doses of 350, 450 and 800 mg/kg, but not at 100 mg/kg; this effect disappeared within the next 15 hours. In addition, a less pronounced erythema was already apparent after irradiation on day 3 at the dose level of 800 mg/kg. However, at time of necropsy, the mice did not show a UV-dependent increase in ear weight at any dose. The ear-draining lymph nodes showed no proliferation response at any dose. Based on the evident erythema reaction, 350 mg/kg was considered to be the lowest observable adverse effect level (LOAEL), while 100 mg/kg may be the no observable adverse effect level (NOAEL).

An alternative design of the UV-LLNA was used at a dose level of 450 mg/kg with the amorphous form in order to address the relevance of daily versus single irradiation (Study D). Mice were administrated three consecutive days with vemurafenib but exposed to simulated sun light only on day 3. Signs of phototoxicity appeared on day 3 directly after UV-exposure, although the ear reddening was reduced compared to the results obtained with the standard study design. As before, no ear weight increase and no proliferation response of the ear-draining lymph nodes were seen at the time of necropsy. This result suggests that for vemurafenib repeated administration is needed in this mouse model in order to induce increased light sensitivity of the skin. Furthermore, induction of lymph node reactions driven by acute ear skin inflammation (as seen, for instance, with sparfloxacin) starts on day 3 and would only become visible after an extension of the treatment protocol up to 5 days.

### 3.3.4. Time-profile of erythema and edema formation after irradiation

The time profile obtained on the last of three consecutive days with daily treatment (Study E, 350 mg/kg amorphous vemurafenib followed by irradiation) is shown in **Figure 3**. Ear weights were significantly increased at 1 h, 2 h, 3 h, 4 h and 6 h post-irradiation compared to the control group, illustrating that a pronounced edema is formed at the same time at which the erythema can be observed. However, 24 hours later (the standard sampling time point of the UV-LLNA) the ear weight increase after vemurafenib had already decreased to pre-dose levels.

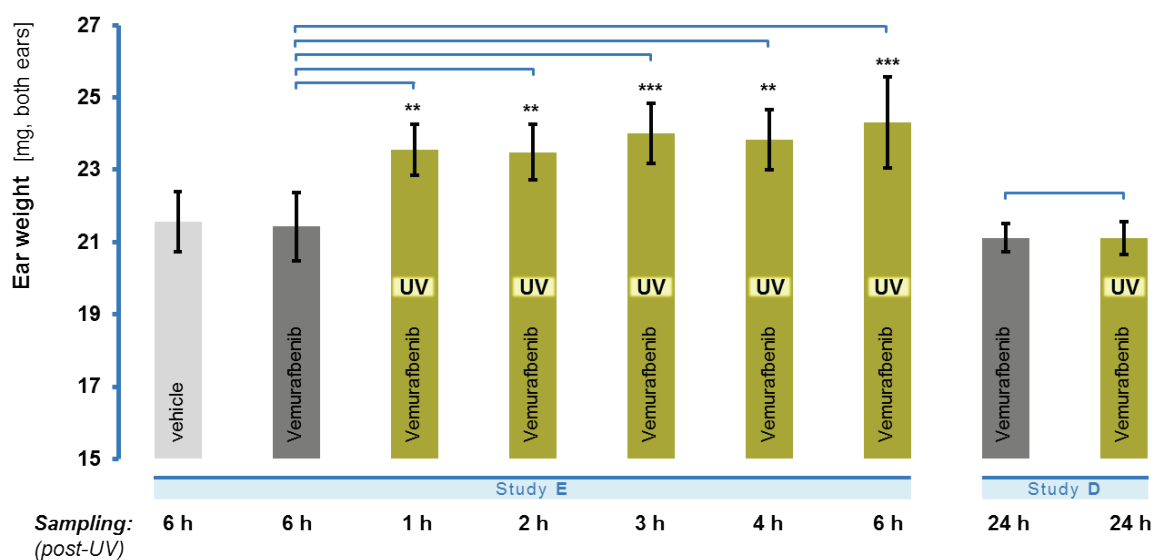


Fig 3. Time-dependent edema reaction in mouse ears. A significant, time-dependent increase (up to 13%) of the ear weights (punch-out biopsies) within 6 hours post-UV exposure is seen. Ear weight at 24 h from Study D. \* Vemurafenib-treated groups (350 mg/kg), comparison UV-exposed *versus* non-UV-exposed. Student's T-Test (unpaired), significance levels: \*\* ( $p < 0.01$ ), \*\*\* ( $p < 0.001$ )

### 3.3.5. Pharmacokinetic Profile

Concentrations of vemurafenib found in mouse plasma over 3 days were found to be similar (**Figure 4**) ranging from 54 to 193  $\mu\text{g/ml}$  ( $C_{\min}$ ,  $C_{\max}$ ) on day 3. The time to reach the highest plasma concentration was between 2 and 4 hours after the administration irrespective of the day. The apparent half-life time was 10 to 13 hours showing a slight decrease during treatment days. The amount of vemurafenib found in ear skin tended to decrease after repetitive administration and was about 2-fold lower compared to plasma. Distinct accumulation was neither found in plasma nor in ear skin.

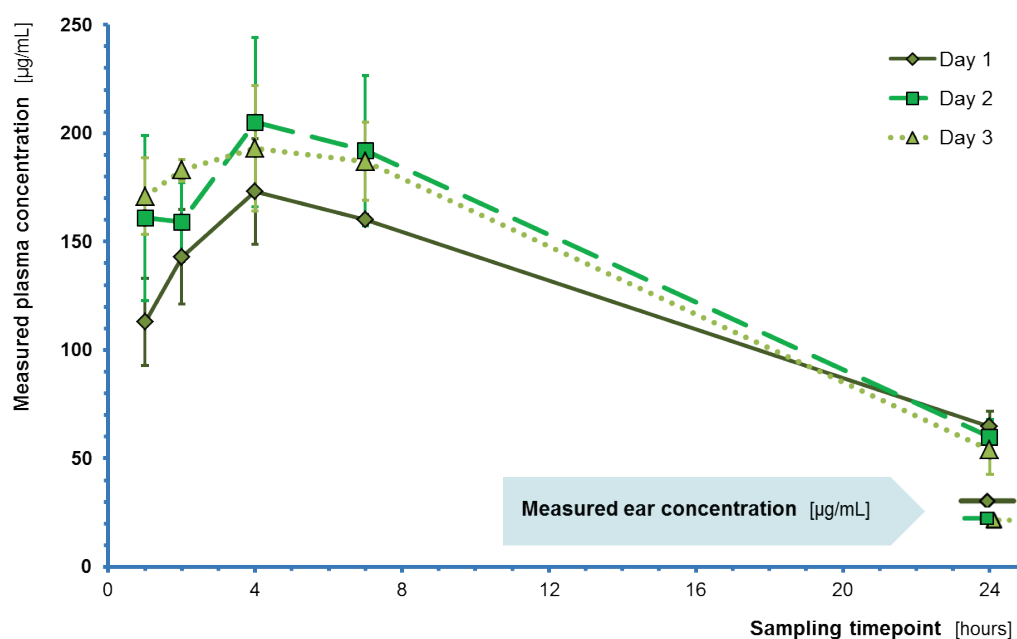


Fig 4. Mean Concentrations of Vemurafenib versus time in mouse plasma. Six mice per group were treated orally with a suspension of amorphous vemurafenib on up to three consecutive days. Blood samples from three animals per time point per group were collected from the vena saphena at 1h, 2h, 4h and 7h post-dose. In addition, from all animals of a group (one per day) terminal samples at 24 h were taken from heart puncture. At the same time point ear samples were taken (punch-out biopsies).

### 3.4. Discussion and Conclusion

From a chemical point of view, vemurafenib carries all features of a clinically relevant phototoxic substance: a) it does absorb sun light within UVB and UVA up to 350 nm; b) it shows *in vitro* a significant phototoxic reaction in cell culture (proving photochemical reactivity) and c) it contains a fundamental structural element (diaryl ketone or benzophenone chromophore) also seen in known clinically phototoxic drugs such as ketoprofen or amiodarone. However, it is important to remember that without sufficient distribution to sun-light exposed tissues such compounds do not lead to clinically relevant phototoxic reactions. Therefore, it is essential to confirm these *in vitro* findings in established animal models of phototoxicity as long as meaningful human phototoxicity data cannot be generated easily.

In our established in-house *in vivo* phototoxicity model (oral UV-LLNA in mice) we were able to demonstrate dose- and time-dependent phototoxicity of vemurafenib using commercially available tablets (stabilized amorphous material). The lowest phototoxic dose was 350 mg/kg given for three consecutive days followed by exposure to UV-visible irradiation at a UVA-normalized dose of 10 J/cm<sup>2</sup> (related blood plasma levels of vemurafenib on day 3, C<sub>max</sub>: 193 µg/ml, C<sub>min</sub>: 54 µg/ml). In comparison, pure vemurafenib, which forms easily crystalline variants and is known to have poor bioavailability, was tested at 350 mg/kg. Indeed, no signs of phototoxicity could be seen, which emphasizes the importance of adequate formulations and confirmed systemic exposure (either measured in blood or tissue or indirectly by clinical signs).

Interestingly, initial studies performed as part of the non-clinical development of vemurafenib could not confirm any phototoxicity *in vivo* (for details see: CHMP review 2011, FDA review 2011). At that time, hairless female rats (Ico:OFA-hr/hr) were treated daily for 7 days at dose levels of 30, 150 and 450 mg/kg using stabilized amorphous material comparable to that used

later in commercial tablets. Although not reported for the hairless rat sufficient systemic exposure can be assumed based on toxicokinetic data available from general toxicity studies (26-week toxicity study, female CrI:CD(SD) rats, daily dose of 450 mg/kg:  $C_{\max}$  at day 1: 70  $\mu\text{g/ml}$ ,  $C_{\max}$  at day 91: 115  $\mu\text{g/mL}$ , converted from reported molar concentrations: 143.1  $\mu\text{M}$  and 234.7  $\mu\text{M}$ , respectively). Irradiation of the treated hairless rats was performed on the last day of treatment starting 90 minutes after last administration of vemurafenib with UVA doses ranging from 5  $\text{J/cm}^2$  to 35  $\text{J/cm}^2$ . The light source had apparently the characteristics of fluorescent tubes with a reported maximal spectral output range from 350 nm to 400 nm and a peak at 370 nm (**Figure 1**). In comparison to the light absorption spectrum of vemurafenib it is becoming evident that there is no spectral overlap between this original light source used during development of vemurafenib and the test compound. This fact alone may fully explain the negative results of this earlier study in hairless rats, since duration of treatment and exposure to both vemurafenib and the formal UVA dose (limited to 350 to 400 nm) was clearly exceeding the conditions we have used in our studies in mice reported above.

In patients efficacious dose levels have been reported to show average  $C_{\max}$  values around 60  $\mu\text{g/mL}$  (CHMP review, 960 mg b.i.d., day 15), which is comparable to the exposure reached in mice at 350 mg/kg and in rats at 450 mg/kg. However, human PK profiles differ significantly from those seen in preclinical animal species. Particularly half-life in blood plasma appears to be several-fold longer in men (57 hours), which suggests that a steady state is reached only after many days of treatment. Nevertheless, it should be noted, that phototoxicity *in vivo* (both animal and human) is driven by the presence of photoreactive molecules in light exposed tissues. Therefore, comparison of achieved peak concentrations ( $C_{\max}$ ) – even at different  $T_{\max}$  – remains the most appropriate exposure assessment (see also ICH S10, 2012) whereas AUC-based evaluations are of limited value.

So far, human phototoxicity data has only been reported from patient populations (see Introduction). Two groups (Dummer 2012, Gerlot 2013) have reported follow-on investigations for individual patients. In summary, clinical representation of vemurafenib-induced phototoxicity was described as a quickly occurring erythema accompanied by an edema and in some cases a burning sensation during light exposure and was apparently UVA dependent. As described by Ferguson (2002) this clinical presentation is typical for direct photochemical mechanisms of phototoxicity. Gerlot et al. speculated that the observed UVA-dependency could be explained by increased systemic porphyrin levels. However, the authors did not discuss the known intrinsic photoreactivity of vemurafenib, which is – as confirmed by our own results – indeed UVA driven (UV-vis spectrum, in vitro and in vivo phototoxicity tests) and can easily explain the clinical reactions. The quick onset of edema formation in mice (**Figure 3**) resembles the acute clinical reactions in men. Although vemurafenib does not show typical signs of accumulation or retention in skin (neither in animals nor in men), phototoxicity may be linked to steady-state conditions. In our in vivo studies an irradiation-induced skin reaction at the lowest effective dose level (350 mg/kg) became apparent only after 3 consecutive days of dosing. However, at higher dose levels these skin reactions started already on day 2. Currently, there is no data providing further insight. Assuming that vemurafenib molecules represent the photoreactive species (rather than endogenous molecules as discussed above), there may be slower but critical redistribution processes (within skin, within cells), which are ultimately driving susceptibility of skin to UVA light.

In conclusion, our investigations on the kinase inhibitor vemurafenib confirm a non-clinical safety profile which is consistent with the clinical signs of phototoxicity seen in many treated patients. Furthermore, these results highlight once again the impact of carefully designed in vivo phototoxicity studies. It is apparent that duration of treatment and timing of irradiation are key parameters to ensure an appropriate sensitivity. These elements of the study design

should be supported by relevant pharmacokinetic data. The common perception is that if a compound presents an identical pharmacokinetic profile over several days, a single-treatment/single-irradiation design is appropriate as it would not be affected by an accumulation of the compound into the skin. However, this case clearly shows that even for compounds without apparent overproportional distribution to skin, a single-treatment/single-irradiation design can be inappropriate. Finally, it is evident that appropriate irradiation conditions are crucial. The more general use of “solar simulator” light sources covering at least the full range of UVA and visible light should be considered state-of-the-art.

## Acknowledgements

We thank Mrs. Monika Spielmann and Mrs. Christine Blumer for their support with the in vitro 3T3 NRU phototoxicity test; Mr. Martin Schneider, Mrs. Nathalie Noll, Mrs. Jeannine Streich, Mr. René Schaffner, Mrs. Déborah Garcia, Mr. Philippe Scheubel and Dr. Jens Schuemann for their expertise and support with the animal experiments; Dr. Frank Picard and Dr. Daniel Neddermann for their support with the pharmacokinetic study; Dr. Ursula Junker for her expertise with the pathology review; Dr. Hans-Joerg Martus and Dr. Willi Suter for their scientific support (all Novartis Pharma AG).

## Funding

This work was supported by Novartis Institute for BioMedical Research, Novartis Pharma AG, Switzerland.

## References

Bollag, G., Hirth, P., Tsai, J., Zhang, J., Ibrahim, P.N., Cho, H., Spevak, W., Zhang, C., Zhang, Y., Habets, G., Burton, E.A., Wong, B., Tsang, G., West, B.L., Powell, B., Shellooe, R., Marimuthu, A., Nguyen, H., Zhang, K.Y., Artis, D.R., Schlessinger, J., Su, F., Higgins, B., Iyer, R., D'Andrea,

- K., Koehler, A., Stumm, M., Lin, P.S., Lee, R.J., Grippo, J., Puzanov, I., Kim, K.B., Ribas, A., McArthur, G.A., Sosman, J.A., Chapman, P.B., Flaherty, K.T., Xu, X., Nathanson, K.L. and Nolop, K. (2010). Clinical efficacy of a RAF inhibitor needs broad target blockade in BRAF-mutant melanoma. *Nature*. **467**(7315):596-9.
- Chapman, P.B., Hauschild, A., Robert, C., Haanen, J.B., Ascierto, P., Larkin, J., Dummer, R., Garbe, C., Testori, A., Maio, M., Hogg, D., Lorigan, P., Lebbe, C., Jouary, T., Schadendorf, D., Ribas, A., O'Day, S.J., Sosman, J.A., Kirkwood, J.M., Eggermont, A.M., Dreno, B., Nolop, K., Li, J., Nelson, B., Hou, J., Lee, R.J., Flaherty, K.T., McArthur, G.A. and BRIM-3 Study Group (2011). Improved survival with vemurafenib in melanoma with BRAF V600E mutation. *N. Engl. J. Med.* **364**:2507–2516.
- Committee for Medicinal Products for Human Use (CHMP) (2011). Assessment Report of Zelboraf, vemurafenib. EMA/CHMP/926998/2011
- Dummer, R., Rinderknecht, J. and Goldinger, S.M. (2012). Ultraviolet A and photosensitivity during vemurafenib therapy. *N. Engl. J. Med.* **366**(5):480-1.
- FDA/Center for Drug Evaluation and Research, Division of Drug Oncology Products (HFD-150) (2011). Pharmacology and Toxicology NDA Review and Evaluation of Zelboraf, vemurafenib.
- Flaherty, K.T., Puzanov, I., Kim, K.B., McArthur, G.A., Sosman, J.A., O'Dwyer, P.J., Lee, R.J., Grippo, J.F., Nolop, K. and Chapman, P.B. (2010). Inhibition of mutated, activated BRAF in metastatic melanoma. *N. Engl. J. Med.* **363**:809–819.
- Ferguson, J. (2002). Photosensitivity due to drugs. *Photodermatol. Photoimmunol. Photomed.* **18**(5):262-9.
- Gelot, P., Dutartre, H., Khammari, A., Boisrobert, A., Schmitt, C., Deybach, J.-C., Nguyen, J.-M., Seit , S. and Dr no, B. (2013), Vemurafenib: an unusual UVA-induced photosensitivity. *Experimental Dermatology*, **22**: 297–298.
- Glantz SA: Primer of Biostatistics, 3rd ed. New York, McGraw-Hill, 1992.

ICH (2012), draft guideline S10 “Photosafety evaluation of pharmaceuticals”,

[http://www.ich.org/fileadmin/Public\\_Web\\_Site/ICH\\_Products/Guidelines/Safety/S10/S10\\_Step\\_2.pdf](http://www.ich.org/fileadmin/Public_Web_Site/ICH_Products/Guidelines/Safety/S10/S10_Step_2.pdf)>.

Lacouture, M.E., Duvic, M., Hauschild, A., Prieto, V.G., Robert, C., Schadendorf, D., Kim, C.C., McCormack, C.J., Myskowski, P.L., Spleiss, O., Trunzer, K., Su, F., Nelson, B., Nolop, K.B., Grippo, J.F., Lee, R.J., Klimek, M.J., Troy, J.L., Joe, A.K. (2013). Analysis of dermatologic events in vemurafenib-treated patients with melanoma. *Oncologist*. **18**(3):314-22.

Mackay, J.M., Elliott, B.M. (1992). Dose ranging and dose settings for in vivo genetic toxicology studies. *Mutat. Res.* **271**:97-99.

OECD (2004), *Test No. 432: In Vitro 3T3 NRU Phototoxicity Test*, OECD Guidelines for the Testing of Chemicals, Section 4, OECD Publishing. doi: "http://dx.doi.org/10.1787/9789264071162-en"10.1787/9789264071162-en"

Shah, N., Iyer, R. M., Mair, H.-J., Choi, D. S., Tian, H., Diodone, R., Fähnrich, K., Pabst-Ravot, A., Tang, K., Scheubel, E., Grippo, J. F., Moreira, S. A., Go, Z., Mouskountakis, J., Louie, T., Ibrahim, P. N., Sandhu, H., Rubia, L., Chokshi, H., Singhal, D. and Malick, W. (2013), Improved human bioavailability of vemurafenib, a practically insoluble drug, using an amorphous polymer-stabilized solid dispersion prepared by a solvent-controlled coprecipitation process. *J. Pharm. Sci.* **102**: 967–981.

Ulrich, P., Streich, J. and Suter, W. (2001). Intralaboratory validation of alternative endpoints in the murine local lymph node assay for the identification of contact allergic potential: primary ear skin irritation and ear-draining lymph node hyperplasia induced by topical chemicals. *Arch. Toxicol.* **74**: 733-744.

Vohr, H.W., Blümel, J., Blotz, A., Homey, B. and Ahr, H.J. (2000). An intra-laboratory validation of the Integrated Model for the Differentiation of Skin Reactions (IMDS): discrimination between (photo)allergic and (photo)irritant skin reactions in mice. *Arch. Toxicol.* Jan; **73**(10-11):501-9.

## 4. Evaluation of Sparfloxacin Phototoxicity with Mass Spectrometry Imaging

[Boudon, S.M., Morandi, G., Prideaux, B., Staab, D., Junker, U., Odermatt, A., Stoeckli, M., Bauer, D. 2013. Evaluation of Sparfloxacin Phototoxicity with Mass Spectrometry Imaging. *JASMS*.] Submitted

**This work was presented at the Gordon Research Conference: Cellular & Molecular Mechanisms of Toxicity. Proctor Academy, Andover, NH, USA, Aug. 2011.** Boudon, S., Schiltz, C., Scheubel, P., Prideaux, B., Luehrs, D., Stoeckli, M., Schuemann, J., Bauer, D. Use of a modified oral UV-LLNA in Balb/c mice for the investigation of phototoxicity mechanisms and pharmacokinetic properties in skin. **Granted the 3<sup>rd</sup> Poster Award.**

**This work was presented at the 14<sup>th</sup> Congress of the European Society for Photobiology, Geneva, Switzerland, Sept. 2011.** Boudon, S., Schiltz, C., Scheubel, P., Prideaux, B., Luehrs, D., Stoeckli, M., Schuemann, J., Bauer, D. Use of a modified oral UV-LLNA in Balb/c mice for the investigation of phototoxicity mechanisms and pharmacokinetic properties in skin.

## Abbreviations

3D	three-dimensional
ACN	acetonitrile
CHCA	$\alpha$ -cyano-4-hydroxycinnamic acid
CMC	carboxymethylcellulose
HBSS	Hank's Balanced Salt solution
MALDI	matrix-assisted laser desorption/ionization
MXF	moxifloxacin
MSI	mass spectrometry imaging
SOP	standard operating procedure
SPX	sparfloxacin
TFA	trifluoroacetic acid
UV	ultraviolet
VIS	visible light

## Abstract

Mass spectrometry imaging (MSI) was applied to samples from mouse skin and from a human in vitro 3D skin model in order to assess the potential advantage of this technique in the context of photosafety evaluation. MSI proved to be a suitable method for the detection of the model compound sparfloxacin in biological tissues following systemic administration (oral gavage) and subsequent exposure to simulated sun light. In the human in vitro 3D skin model, a concentration-dependent increase as well as an irradiation-dependent decrease of sparfloxacin in tissue samples was observed. The MSI data on samples from mouse skin showed high concentrations of sparfloxacin 8 hours after dosing. In contrast, animals irradiated with simulated sun light showed a significant lower tissue exposure starting already at 1 hour post-irradiation, with no measurable intensity at the later time points (3 hours and 6 hours), suggesting a time- and irradiation-dependent degradation of sparfloxacin. The resolution of 100  $\mu\text{m}$  proved to be adequate for the resolution of a total tissue concentration, but higher resolutions beyond 10  $\mu\text{m}$  would be required to resolve tissue structures. The detection of sparfloxacin parent compound was apparently only the first step in an attempt to gain a deeper understanding of the phototoxic processes. Further work is needed to identify the degradation products of sparfloxacin implicated in the observed inflammatory processes in order to better understand the origin and the mechanism of the phototoxic reaction.

## 4.1. Introduction

Phototoxic properties of pharmaceutical products may cause serious adverse drug reactions. This does not only apply to ultraviolet (UV) and/or visible (vis) light absorbing chemicals, which are used topically, but also to those which reach light-exposed tissues such as skin or eyes following systemic exposure (for review see Drucker and Rosen, 2011; Ferguson, 2002; Moore, 2002).

To enhance our molecular understanding of phototoxicity mechanisms, matrix-assisted laser desorption/ionization mass spectrometric imaging (MALDI-MSI) was applied to samples from mouse skin and from a human 3D skin model in order to assess the potential advantage of this technique in the context of photosafety evaluation.

Since its introduction over 10 years ago (Caprioli et al, 1997), MALDI-MSI has emerged as a valuable method of mapping the distribution of compounds and metabolites in animal tissues after dosing (Steockli et al, 2007; Rohner et al, 2005; Trim et al, 2008). It offers the distinct advantage compared to alternative molecular imaging techniques of allowing label-free and simultaneous detection of hundreds of molecules in a single experiment. This makes it the method of choice for applications to investigate molecular effects in combination with substance dosing, or to measure multiple substances simultaneously. As an example, the strength of mass spectrometry imaging was demonstrated by analyzing the distribution of multiple fluoroquinolones in lung tissue of tuberculosis infected rabbits (Prideaux et al, 2011).

Based on these findings, the phototoxic effects of sparfloxacin, an antibiotic drug belonging to the class of fluoroquinolones and a well-known photosensitizer in human (Pierfitte et al,

2000), were analyzed in the present study. We aimed to spatially follow the substance and its metabolites, as well as molecular changes, in the tissue following the treatment.

*In vitro* 3D human skin models represent a simplified system for studying the interaction between irradiation with simulated sun light and human skin at both the cellular and molecular levels. In this study, we used the Phenion® Full Thickness Skin Model which consists of keratinocytes and fibroblasts and presents an epidermis, a basement membrane and a dermis featuring morphology and tissue functionality very close to the characteristics of human skin (Ackermann et al, 2010).

Furthermore, starting from an established *in vivo* phototoxicity model (Boudon et al., 2013; Schuemann et al. 2014), the study design was supplemented with early sampling time points of typical light exposed tissues. Balb/c mice were treated orally with sparfloxacin and subsequently irradiated with simulated sun light in order to establish time-dependent profiles for both inflammatory responses (erythema, edema, histopathological changes) and presence of sparfloxacin in these tissues.

## 4.2. Materials and methods

### 4.2.1. Human 3D skin model

The Phenion® FT model (Henkel, Düsseldorf, Germany) is a multilayered equivalent of the human skin. It has a diameter of 1.3 cm and consists of keratinocytes and fibroblasts derived from the same human donor. The tissue pieces were handled according to the instructions of the manufacturer. Immediately after arriving each specimen of the FT model was transferred from the delivery plate into a 3.5-cm Petri dish equipped with filter paper and filled with

approximately 4–5 ml of preheated culture medium (37°C, Air Liquid Interface Medium). Tissue pieces were then incubated overnight at 37°C, with 5% CO<sub>2</sub> and saturated humidity. Three concentrations of sparfloxacin were used: 1 µg/mL, 3 µg/mL and 10 µg/mL in HBSS (Hank's Balanced Salt solution) that were added to the Air Liquid Interface medium in order to mimic the systemic distribution from blood to dermis and epidermis. After an overnight incubation with sparfloxacin some of the treated tissue cultures were exposed to simulated sun light (10 J/cm UVA, SOL500, Dr. Höhnle, Germany) during 1 hour with an intensity of 2 mW/cm<sup>2</sup>. 8 h later all tissues were processed for bioanalytical analyses. Each skin sample was cut into two half, one was snap-frozen and the other one fixed in formalin and embedded in paraffin.

## 4.2.2. Animal experiments

### 4.2.2.1. Animal husbandry

Female Balb/c mice aged of about 8 weeks at start of experiment purchased from Charles River (France) were acclimatized for around one week. The experiments were performed in conformity with the Swiss Animal Welfare Law and in accordance with internal SOPs and guidelines for care and use of laboratory animals. Animals had ad libitum access to pelleted standard rodent diet and tap water from the domestic supply and were kept in an air-conditioned animal room under periodic bacteriological control, at 22°C ± 2°C with monitored 40% - 80% humidity, a 12 hours light/dark cycle and background radio coordinated with light hours.

#### 4.2.2.2. Irradiation conditions for animal experiments

During irradiation mice were kept in specific cages allowing only for lateral movements and ensuring a uniform irradiation of their backs and ears. Non-irradiated animals were kept in their housing cages under standard room light. Six mice per group were exposed to simulated sun light (Psorisan 900 H1 lamp; Dr. Hönle, Germany) with a main spectral output from 320 until beyond 590 nm. Typically, the applied intensity was  $4.8 \text{ mW/cm}^2$  at a distance of 50 cm. Irradiation was normalized to a dose of  $10 \text{ J/cm}^2$  UVA. The integrated H1 filter system attenuated the highly cytotoxic UVB range to a level which was tolerated by the animals. This adjustment is recommended for testing oral drugs, since in such cases photosafety assessment is mainly focusing on UVA and visible light as only these wavelengths are penetrating sufficiently into skin (ICH S10, 2013). UVA irradiance was measured with a UV radiometer (Gigahertz-Optik GmbH, Germany). The yearly calibration of this GLP-compliant equipment with an externally calibrated spectroradiometer covering the full spectral range from 250 to 800 nm was performed by opto.cal GmbH (Switzerland). The timing for exposure to simulated sun light was based on the pharmacokinetic properties and started one hour after dosing. Corresponding control groups treated with vehicle, not exposed to simulated sun light, were included.

#### 4.2.2.3. Treatment protocols

Groups of six mice were used for single-dose oral gavage administration. Two groups remained unirradiated and were euthanized 8 hours post-treatment: one group treated with 100 mg/kg sparfloxacin in 0.5% aqueous carboxymethylcellulose (CMC) and one group treated with vehicle alone. Four groups were treated with the test item as well but followed

by exposure to simulated sun light one hour after treatment. These mice were euthanized 1, 2, 3, 4 and 6 hours post-irradiation. Circular biopsies ( $0.5 \text{ cm}^2$ ) from the apical area of each ear were excised using a disposable punch, weighed as pairs on analytical scales and further processed for histopathological and bioanalytical analyses. For each animal, one ear was snap-frozen and the other one fixed in formalin and embedded in paraffin. Ear samples excised twenty-four hours post-irradiation, obtain from another study, were added for comparison.

#### 4.2.2.4. Statistical analysis

For all statistical calculations SigmaPlot for Windows (version 11.0) was used. A One-Way-Analysis-of-Variance was used as the statistical method (Glantz SA, 1992). A normality test was performed to assure that the specimens were drawn from a normal population (significance level = 0.01). The equal variance test was used to check the assumption that the sample was drawn from populations with the same variance (significance level = 0.01). In case of significant results of the One-Way-ANOVA, multiple comparisons were performed with the Student-Newman-Keuls test. If the normality test and/or the equal variance test gave  $p$  values  $< 0.01$ , a suitable transformation (log, square root) was applied; if the normality test and/or equal variance test still gave  $p$  values  $< 0.01$ , the non-parametric Kruskal-Wallis test was used and multiple comparisons for the ranks of the original observations were performed. The confidence interval for the difference of the means was set to 95% ( $\alpha = 0.05$ ).

### 4.2.3. Mass spectrometry imaging

#### 4.2.3.1. Preparation of tissue samples for MALDI-MSI

Frozen ear biopsies were mounted on a holder without embedding by using small amounts of O.C.T. (Optimum Cutting Temperature Tissue-Tek, Sakura Finetek, Torrance, USA) and sections were cut at 12  $\mu\text{m}$  thickness using a cryotome (CM3050, Leica Microsystems, Wetzlar, Germany). The sections were thaw-mounted on stainless steel carrier, carefully avoiding contamination of the sample and plate with O.C.T. At least three sections per sample were prepared using the above protocol. Once sectioned, the samples were stored at  $-80^{\circ}\text{C}$  until further analysis. Alternating sections for each biopsy were cut and mounted onto glass microscope slides and subject to tissue fixation and hematoxylin and eosin staining. Dehydration of the sections was achieved by rapidly transferring the stainless steel targets containing the tissues from the freezer to a desiccator. After 15 min desiccation, the plates were scanned using a flatbed scanner (HP Scanjet 6300C) with a resolution of 10  $\mu\text{m}$ . The MALDI matrix was applied to the plates as a solution of 10 mg/mL  $\alpha$ -cyano-4-hydroxycinnamic acid (CHCA, C8982, Sigma) in 50% acetonitrile (ACN) containing 0.1% trifluoroacetic acid (TFA). Moxifloxacin (MFX) (Sigma, Buchs, Switzerland), another member of the groups of fluoroquinolones, was added as internal standard in a stock solution of 1 nmol/ $\mu\text{L}$  (50% ACN) to produce a final concentration in the matrix solution of 2 pmol/ $\mu\text{L}$ . Eight mL of matrix/MFX standard solution were applied to each plate using a TLC sprayer (VWR, Dietikon, Switzerland) operated at 0.5 bar pressure and held at a distance of 20 cm from the plate. Approximately 30 passes were performed per plate with 30 s drying time between cycles.

#### 4.2.3.2. MALDI-MSI analysis

Standard solutions of sparfloxacin (Sigma, Buchs, Switzerland) and moxifloxacin were analyzed using a FlashQuant mass spectrometer (AB Sciex, Toronto, CA) to establish a SRM method for each substance. Instrument parameters were optimized for highest product ion signal in both analytes. Product ion scans of the protonated precursor ions ( $m/z$  393.2 SPX) revealed a clear fragmentation pattern with the transition  $m/z$  393.2  $\rightarrow$  375.2 dominating the spectra and which was selected for the analysis. Increasing the laser power and collision energy resulted in a greater range of product ions produced but significantly reduced sensitivity.

Image acquisition was achieved by using the FlashQuant 1.1 beta imaging software (AB Sciex) and running the ND:YAG laser at 1 kHz. The instrument was operated in selected reaction monitoring (SRM) mode monitoring the established positive fragment ions with the laser rastering across the tissue at a continuous scan speed of 1.5 mm per second and at a line distance of 100  $\mu$ m in a serpentine pattern. This method setup resulted in a dwell time of 50 ms for each of the two transitions. Both Q1 and Q3 were set to transmit a 1 Da window centered on the specific masses. Image acquisition windows varied in size between 1  $\times$  1 cm and 2  $\times$  2 cm depending upon the dimensions of the biopsy section, and image acquisition time was approximately 30 minutes per tissue section depending on the image area.

In-house-developed software (Stoeckli, Novartis, Switzerland) was used to convert the standard FlashQuant data format (.wiff) into the BioMap readable Analyze 7.5 format (Mayo Foundation, Rochester, MN). BioMap (Novartis, Basel, Switzerland) was used for data processing and visualization. Result images were calculated by dividing the pixel intensities of the compound by the one of the added internal standard.

## 4.3. Results and discussion

### 4.3.1. Localization and quantification of sparfloxacin in vitro

The optimized mass spectrometric imaging method allowed high signal intensities for all sample conditions and obtained images showed a good contrast (**Figure 1**). The normalization, selected by an internal standard, compensated for the differences in sample preparation conditions and allowed a direct and absolute comparison between the image data sets. A pronounced concentration-dependent increase of sparfloxacin concentrations was observed from 1  $\mu\text{g/mL}$ , over 3  $\mu\text{g/mL}$  to 10  $\mu\text{g/mL}$  in the MS images. In comparison, a significant decrease in sparfloxacin intensity was observed at all time-points in images of tissues irradiated with simulated sun light. While the spatial resolution of 100  $\mu\text{m}$  provided enough data points for an evaluation of the total tissue concentration, it did not allow for an unambiguous correlation of the signal intensities to specific structures and cell types of the tissue.

### 4.3.2. Localization and quantification of sparfloxacin as part of an in vivo phototoxicity study in mice

In vehicle or sparfloxacin-treated groups no signs of inflammation were seen without exposure to simulated sun light (**Figure 2**). However, following sparfloxacin treatment and subsequent irradiation, edema, congestion and inflammatory infiltrate (granulocytes, neutrophils) became evident confirming the concomitantly observed erythema. While groups sacrificed at 2 hours and 4 hours after irradiation showed an acute reaction, edema and congestion were less prominent in groups sacrificed at 6 hours and 24 hours.

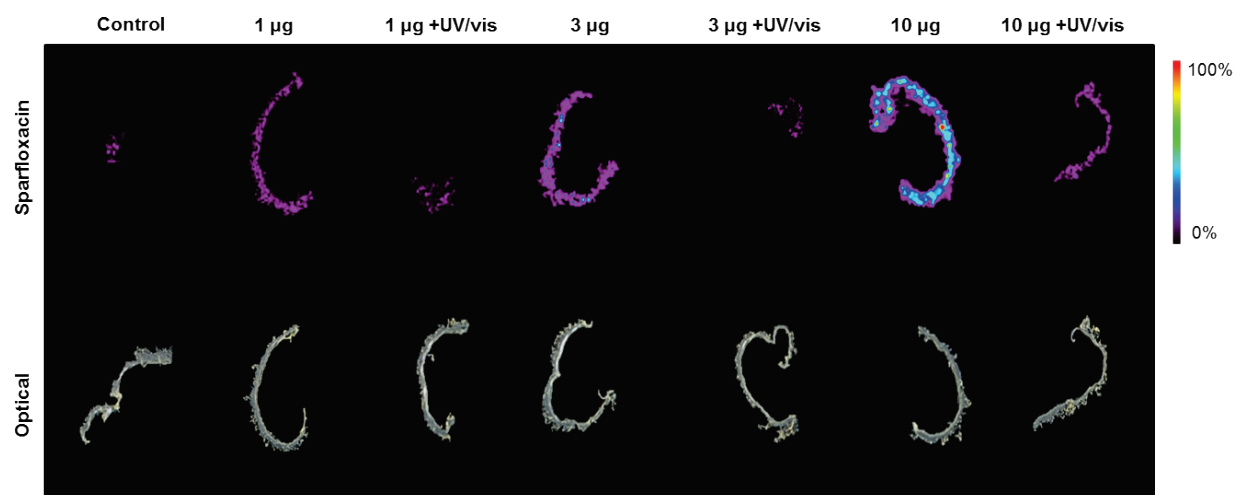


Fig 1. Concentration- and irradiation-dependent sparfloxacin exposure of the in vitro 3D human skin model. Phenion® tissue pieces treated with different concentration of sparfloxacin and partially irradiated with simulated sun light were analyzed by mass spectrometry imaging (MALDI-SRM-QqQ) in order to provide quantitative localization data. A subsequent reference tissue section is displayed below these images. A concentration-dependent increase and an irradiation-dependent decrease of sparfloxacin in tissues was observed. Data shown are the transitions of  $m/z$  393.2 to  $m/z$  375.2 normalized by the SRM intensity of moxifloxacin, being added as internal standard during the CHCA matrix application. Same absolute intensity scale for all images. MS images: 100  $\mu\text{m}$  pixel size. Scale bar: 500  $\mu\text{m}$ .

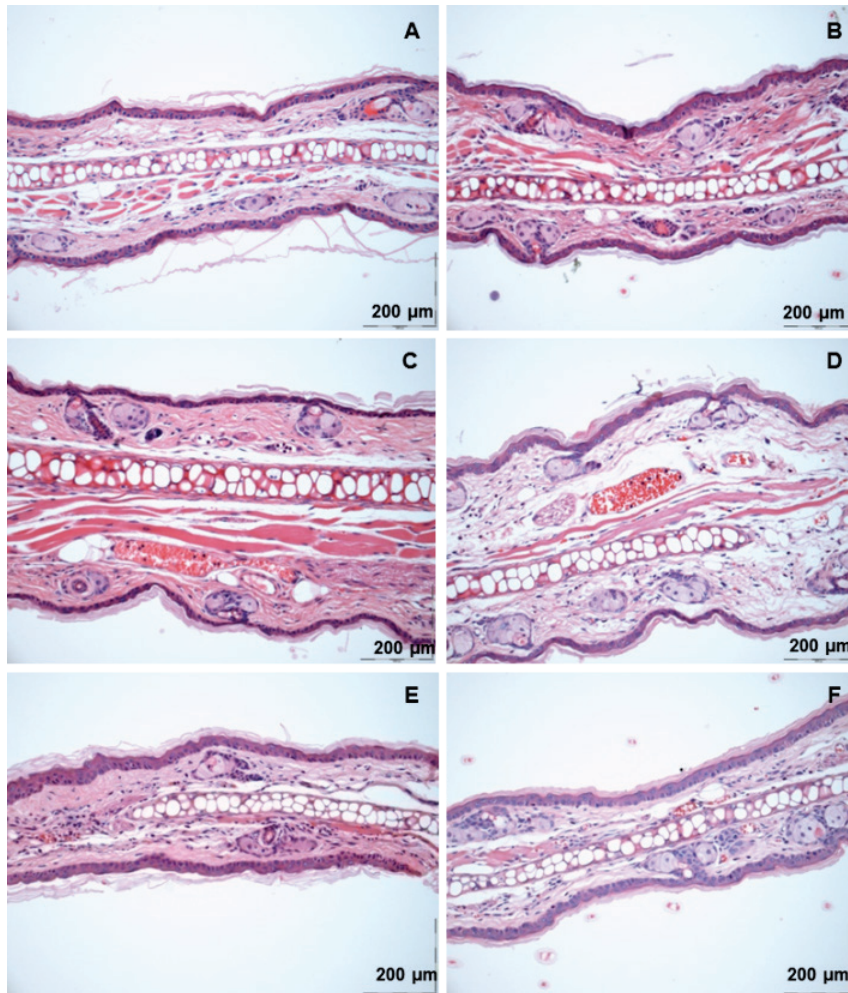


Fig 2. Hematoxylin & Eosin staining of mouse ears. Time and irradiation-dependent edema and congestion reactions following oral (gavage) administration of sparfloxacin 100 mg/kg to female Balb/c mice at two (C), four (D), six (E) and twenty-four (F) hours post-irradiation compared to vehicle (A) and non-irradiated animals (B).

The time-dependent edema reaction seen with 100 mg/kg sparfloxacin followed by irradiation is shown in **Figure 3**. Ear weights were significantly increased at 2 hours, 3 hours and 4 hours post-irradiation compared to the control group, confirming that a pronounced edema was formed at the same time at which the erythema was observed. However, 6 hours later the ear weight had already decreased.

The MSI data showed high concentrations of sparfloxacin at 8 hours after dosing (non-irradiated group administered and scarified in parallel to the 6 hours post-irradiation group)(Figure 4, without UV/vis). In contrast, animals exposed to simulated sun light showed significantly lower tissue concentrations already at 1 hour post-irradiation, with no measurable intensity at the later time points (3 and 6 hours). Images acquired from control animals were added to demonstrate the specificity of the applied MS/MS transition and confirmed the validity of the observed results. Again, the spatial resolution of 100  $\mu\text{m}$  provided enough data points for an evaluation of the total tissue concentration. However, it did not allow for an unambiguous correlation of the signal intensities to specific structures and cell types of the tissue.

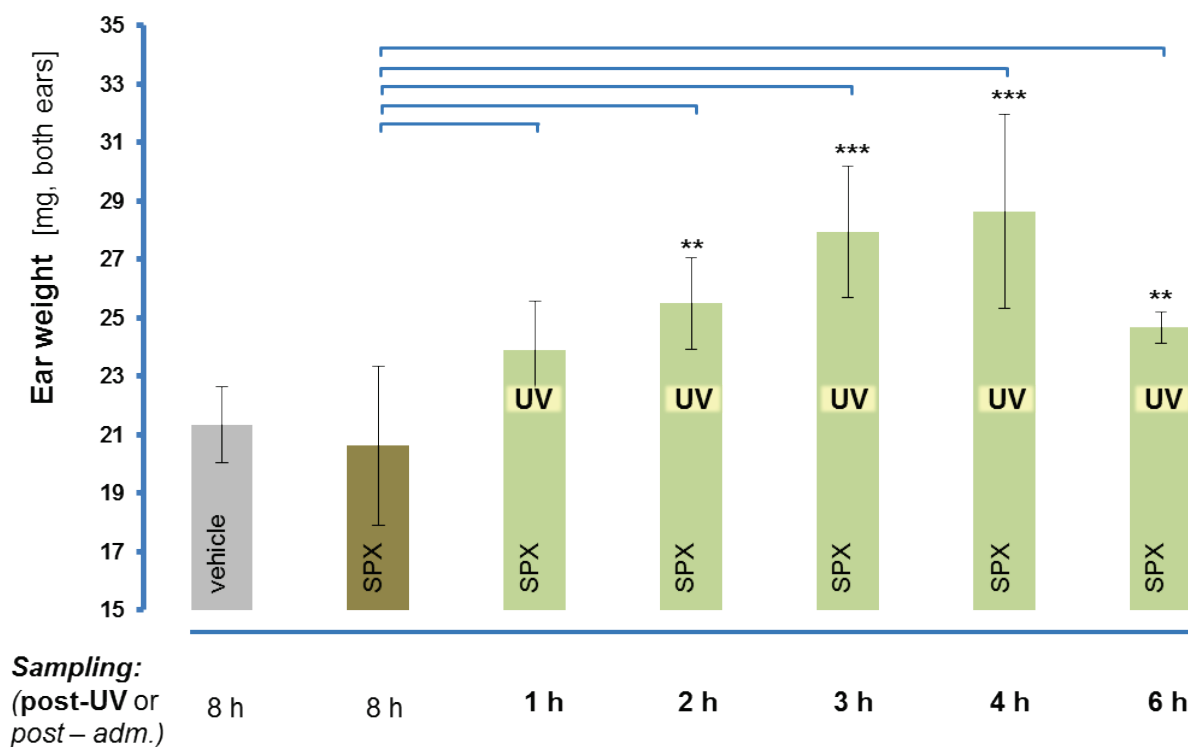


Fig 3. Time-dependent edema reaction in mouse ears. A significant, time-dependent increase of the ear weights at 2 hours (20%), at 3 and 4 hours (more than 30%) post-UV/vis irradiation is seen, which decreases at 6 hours.

\* Sparfloxacin-treated groups (SPX, 100 mg/kg), comparison UV/vis-irradiated *versus* non-UV/vis-irradiated.

*Student's T-Test (unpaired), significance levels: \*\* ( $p < 0.01$ ), \*\*\* ( $p < 0.001$ )*

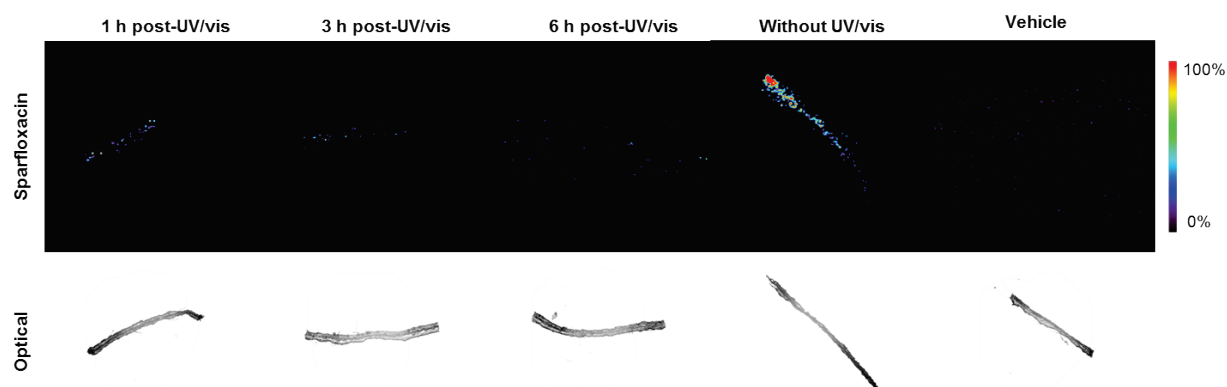


Fig 4. Time course of sparfloxacin distributions in mouse ears after treatment and subsequent irradiation with simulated sun light. Mass spectrometric imaging (MALDI-SRM-QqQ) profile on ear samples from oral (gavage) administration of sparfloxacin 100 mg/kg to female Balb/c mice at 1, 3 and 6 hours post-irradiation compared to vehicle and non-irradiated animals. MS images show high exposure to sparfloxacin 8 hours after dosing (without UV/vis). In contrast, animals irradiated with simulated sun light showed a significantly lower tissue exposure illustrating a time- and irradiation-dependent MSI profile. Subsequent reference tissue sections are displayed below these respective images. Setup: FlashQuant QTRAP mass spectrometer (AB Sciex), fitted with a 1kHz ND:YAG laser. Data shown are the transition of  $m/z$  393.2 to  $m/z$  375.2 normalized by the SRM intensity of MFX, being added as internal standard during the CHCA matrix application. Same absolute intensity scale for all images. MS images: 100  $\mu\text{m}$  pixel size. Scale bar: 500  $\mu\text{m}$ .

## 4.4. Conclusion

In the context of photosafety evaluation, MSI proved to be a suitable method for the detection of photoreactive compounds in biological tissue samples. Using sparfloxacin as a model compound, concentration-dependent and irradiation-dependent effects could be observed in vitro. Furthermore, in an established in vivo phototoxicity model, time- and irradiation dependent exposure to sparfloxacin in skin samples from mouse ears following oral treatment were demonstrated.

Obviously, the detection of the parent compound was only the first step in an attempt to gain a deeper understanding of the phototoxic processes. Identification of degradation products or adducts formed with biological matrix molecules would help better understand the pathways of light-induced photoreactivity within a cellular environment. Likewise, improved resolution at least similar to light microscopy would allow for a direct comparison with changes seen in histopathological evaluations. However, in both cases such improvements will depend on further progress made on the technology level.

## Acknowledgements

We thank Mr. Martin Schneider and Dr. Ulla Plappert-Helbig for their expertise and support with the animal experiments; Dr. Hans-Joerg Martus and Dr. Willi Suter for their scientific support (all Novartis Pharma AG).

## References

Ackermann, K.; Lombardi Borgia, S.; Korting, H.C.; Mewes, K.R.; Schäfer-Korting, M. The Phenion

- full-thickness skin model for percutaneous absorption testing. *Skin Pharmacol Physiol.* **2010**, *23*, 105–112
- Boudon S.M., Plappert U., Odermatt A., Bauer D. 2013. Characterization of vemurafenib's phototoxicity in a mouse model. 2013. *Toxicol. Sci.* Advance Access published October 23, 2013 doi:10.1093/toxsci/kft237
- Caprioli, R. M.; Farmer, T. B.; Gile, J. Molecular imaging of biological samples: localization of peptides and proteins using MALDI-TOF MS. *Anal. Chem.* **1997**, *69*, 4751–4760
- Drucker, A.M.; Rosen, C.F. Drug-induced photosensitivity. *Drug Saf.* **2011**, *34*, 821-837.
- Ferguson, J. Photosensitivity due to drugs. *Photodermatol. Photoimmunol. Photomed.* **2002**, *18*, 262-269.
- Moore, E.M. Drug-induced cutaneous photosensitivity. *Drug Saf.* **2002**, *25*, 345-372.
- Pierfitte, C.; Royer, R.J.; Moore, N.; Bégaud, B. The link between sunshine and phototoxicity of sparfloxacin. *Br J Clin Pharmacol.* **2000**, *49*(6), 609–612.
- Prideaux, B.; Dartois, V.; Staab, D.; Weiner, D.M.; Goh, A.; Via, L.E.; Barry, C.E. 3<sup>rd</sup>; Stoeckli, M. High-sensitivity MALDI-MRM-MS imaging of moxifloxacin distribution in tuberculosis-infected rabbit lungs and granulomatous lesions. *Anal Chem.* **2011**, *83*(6), 2112-8.
- Rohner, T. C.; Staab, D.; Stoeckli, M. MALDI mass spectrometric imaging of biological tissue sections. *Mech. Ageing Dev.* **2005**, *126*, 177–185
- Stoeckli, M.; Staab, D.; Schweitzer, A. Imaging of a beta-peptide distribution in whole-body mice sections by MALDI mass spectrometry. *Int. J. Mass Spectrom.* **2007**, *260*, 195–202
- Trim, P. J.; Henson, C. M.; Avery, J. L.; McEwan, A.; Snel, M. F.; Claude, E.; Marshall, P. S.; West, A.; Princiville, A. P.; Clench, M. R. Matrix-assisted laser desorption/ionization-ion mobility separation-mass spectrometry imaging of vinblastine in whole body tissue sections. *Anal. Chem.* **2008**, *80*, 8628–8634.
- [Schuemann J., Boudon S., Loll N., Garcia D., Schaffner R., Streich J., Ulrich P., Kittel B. and Bauer D. 2013. Integrated preclinical photosafety testing strategy for systemically applied pharmaceuticals. *Toxicology.*] – Submitted

## 5. Conclusion and Perspectives

In this work, we were interested in comparing the results obtained in nonclinical models (*in vitro* and *in vivo* experiments) with the clinical signs observed in human of well-known photosensitizer.

The clinically phototoxic compounds sparfloxacin, enoxacin, lomefloxacin, doxycycline and vemurafenib were reliably identified as phototoxic in the modified murine UV-LLNA in a dose-dependent manner.

The *in vivo* phototoxic potential of systemically applied promethazine and ketoprofen proved to be more difficult to identify. While promethazine did not show a phototoxic potential in the modified murine photo-LLNA up to a dose of 100 mg/kg/day (maximum tolerated dose), ketoprofen could only be identified based on erythema formation at the toxic dose level of 500 mg/kg/day. These results correlate well with the clinically observed difference of ketoprofen-associated phototoxicity risks following topical vs systemic administration and highlight the importance of a careful evaluation of the incidence and relevance of phototoxicity seen clinically after oral administration.

Sparfloxacin and doxycycline induced moderate erythema formation within five to six hours after the first treatment depending on additional exposure to simulated sun light. The severity and persistence of erythema formation increased over the following two days of treatment dose-dependently.

However, vemurafenib-induced erythema formation appeared only after the third treatment and within the six hours following exposure to simulated sun light. In addition, our results demonstrate that the phototoxic potential of vemurafenib was clearly detectable *in vivo* provided that appropriate irradiation conditions were selected.

These results illustrate important lessons regarding photosafety testing.

- First, they demonstrate that the modified murine UV-LLNA, based on quantification of skin irritation (erythema, ear biopsy weight) and auricular LN hyperplasia, is suitable to support preclinical photosafety assessment of systemically applied drug candidates.
- Furthermore, these results highlight the impact of carefully designed *in vivo* phototoxicity studies.
  - It is apparent that duration of treatment and timing of irradiation are key parameters to ensure an appropriate sensitivity. These elements of the study design should be supported by relevant pharmacokinetic data. The common perception is that if a compound presents an identical pharmacokinetic profile over several days, a single-treatment/single-irradiation design is appropriate as it would not be affected by an accumulation of the compound into the skin. However, vemurafenib's case clearly shows that even for compounds without apparent overproportional distribution to skin, a single-treatment/single-irradiation design can be inappropriate.

- It is also evident that appropriate irradiation conditions are crucial. The general use of “solar simulator” light sources covering at least the full range of UVA and visible light should be considered state-of-the-art.
- The inclusion of three dose levels supports the establishment of NOAELs and LOAELs. This allows the calculation of safety margin between drug exposure, which is not associated with signs of phototoxicity *in vivo*, and exposure levels in animal or men, which is considered pharmacologically relevant.

In the context of photosafety evaluation, mass spectrometric imaging (MSI) proved to be a suitable method for the detection of photoreactive compounds in biological tissue samples. Using sparfloxacin as a model compound, concentration-dependent and irradiation-dependent effects could be observed *in vitro*. Furthermore, in an established *in vivo* phototoxicity model, time- and irradiation dependent exposure to sparfloxacin in skin samples from mouse ears following oral treatment were demonstrated. In light of these promising results, MSI was also applied to skin samples from the aforementioned UV-LLNA with vemurafenib and doxycycline (data not shown). Unfortunately, the limit of detection was too low and it was not possible to detect the compounds signal into the mouse ears samples. This illustrates the current limits of MALDI-MSI. This approach is only applicable to molecules that are ionizable by the MALDI process and the sensitivity therefore depends on the molecular nature of targeted compound.

Our described MSI approach was primarily focused on the detection of the parent compound in an attempt to gain a deeper understanding of the phototoxic processes. However, the identification of degradation products or adducts formed with biological matrix molecules would help better understand the pathways of light-induced photoreactivity within a cellular

environment. Likewise, improved resolution at least similar to light microscopy would allow for a direct comparison with changes seen in histopathological evaluations. However, localization and quantification of inflammation markers in skin sections collected during the first hours after irradiation remains challenging. Thus, in both cases, MSI and histopathology, such improvements will depend on further progress made on the technology level.

In conclusion, this work has provided critical scientific results which clearly demonstrate the relevance of certain key elements in an integrated photosafety testing strategy. Apparently, a better understanding towards the behavior of phototoxic drug substances on the molecular level still remains a challenge and should deserve more efforts.



